Missense Mutations in the Human Nanophthalmos Gene *TMEM98* Cause Retinal Defects in the Mouse

Sally H. Cross[1]*, Lisa Mckie[1], Margaret Keighren[1], Katrine West[1], Caroline Thaung[2,3], Tracey Davey[4], Dinesh C. Soares[1,5], Luis Sanchez-Pulido[1] and Ian J. Jackson[1]

[1]MRC Human Genetics Unit, MRC Institute of Genetics and Molecular Medicine, University of Edinburgh, Crewe Road, Edinburgh EH4 2XU, United Kingdom

[2]Moorfields Eye Hospital NHS Foundation Trust, 162 City Road, London EC1V 2PD, United Kingdom.

[3]UCL Institute of Ophthalmology, 11-43 Bath Street, London EC1V 9EL, United Kingdom.

[4]Electron Microscopy Research Services, Newcastle University, Newcastle NE2 4HH, United Kingdom.

[5]current address ACS International Ltd., 267 Banbury Road, Oxford OX2 7HT, United Kingdom

*corresponding author Email: sally.cross@igmm.ed.ac.uk Tel: +44 131 651 8500

Running Title: Human *TMEM98* Nanophthalmos Mutations in the Mouse

ABSTRACT

PURPOSE. We previously found a dominant mutation, *Rwhs*, causing white spots on the retina accompanied by retinal folds. Here we identify the mutant gene to be *Tmem98.* In humans, mutations in the orthologous gene cause nanophthalmos. We modelled these mutations in mice and characterised the mutant eye phenotypes of these and *Rwhs*.

METHODS. The *Rwhs* mutation was identified to be a missense mutation in *Tmem98* by genetic mapping and sequencing. The human *TMEM98* nanophthalmos missense mutations were made in the mouse gene by CRISPR-Cas9. Eyes were examined by indirect ophthalmoscopy and the retinas imaged using a retinal camera. Electroretinography was used to study retinal function. Histology, immunohistochemistry and electron microscopy techniques were used to study adult eyes.

RESULTS. An I135T mutation of *Tmem98* causes the dominant *Rwhs* phenotype and is perinatally lethal when homozygous. Two dominant missense mutations of *TMEM98*, A193P and H196P are associated with human nanophthalmos. In the mouse these mutations cause recessive retinal defects similar to the *Rwhs* phenotype, either alone or in combination with each other, but do not cause nanophthalmos. The retinal folds did not affect retinal function as assessed by electroretinography. Within the folds there was accumulation of disorganised outer segment material as demonstrated by immunohistochemistry and electron microscopy, and macrophages had infiltrated into these regions.

CONCLUSIONS. Mutations in the mouse orthologue of the human nanophthalmos gene *TMEM98* do not result in small eyes. Rather, there is localised disruption of the laminar structure of the photoreceptors.

INTRODUCTION

43

44 There are a range of genetic disorders which present with a reduced eye size. In

45 microphthalmia the reduced size is often associated with additional developmental eye

46 defects, such as coloboma, and may also include developmental defects in other organs. In

47 some cases there is an overall size reduction without other developmental defects. The

48 smaller eye may be a result of a reduction in size of the anterior segment alone (anterior

49 microphthalmos), the posterior segment alone (posterior microphthalmos) or a reduction of

50 both. This last category includes simple microphthalmos and the more severe

51 nanophthalmos [1, 2]. Posterior microphthalmos is sometimes considered as part of a

52 continuum with nanophthalmos, as they have pathological and genetic features in common.

53 In nanophthalmos eye length is reduced by 30% or more, and is usually associated with

54 other ocular features, notably a thickened choroid and sclera, as well as a high incidence of

55 glaucoma, corneal defects, vascular defects and a range of retinal features including retinitis

56 pigmentosa, retinoschisis, retinal detachments and retinal folds. Retinal folds are also

57 observed in posterior microphthalmos, and are sometimes ascribed to a relative overgrowth

58 of neural retina within a smaller globe, resulting in folding of the excess retinal tissue.

59 A number of genes have been found to be associated with nanophthalmos [2]. Mutations in

60 three genes have established associations with nanophthalmos. Several families with

61 nanophthalmos have been found to have clear loss of function mutations in both alleles of

62 the gene encoding membrane-type frizzled related protein, *MFRP*, that is expressed

63 principally in the RPE and ciliary body [3]. Homozygous loss of function mutations in *MFRP*

64 have been found in other individuals with posterior microphthalmia plus retinitis pigmentosa,

65 foveoschisis and drusen, indicating likely genetic background effects on the severity or range

66 of the disease [4-6]. A second autosomal recessive nanophthalmos gene is *PRSS56*, encoding

67 a serine protease. Families with biallelic mutations in this gene have been characterised,

68 some of whom have posterior microphthalmia whilst others have nanophthalmos [7-9]. There is

69 no apparent genotype-phenotype correlation; there are patients with homozygous frameshift

70 mutations with either condition. Intriguingly, association of variants at *PRSS56* with myopia

71 has been reported in genome-wide association studies [10, 11].

72 Most recently three families have been characterised in which heterozygous mutations in

73 *TMEM98* are segregating with nanophthalmos. Two families have missense mutations, the

74 third has a 34bp deletion that removes the last 28 bases of exon 4 and the first six bases of

75 intron 4 including the splice donor site[12, 13]. The effect of the deletion on the *TMEM98*

3

76   transcript is unknown but *in silico* splicing prediction programs (Alamut Visual Splicing

77   Predictions) predict that it could result in exon 4 being skipped, and the production of a

78   potentially functional protein with an internal deletion. Alternatively, other splice defects

79   would result in frameshifts, nonsense mediated decay and loss of protein from this allele. In

80   this case the cause of the disease would be haploinsufficiency. Caution in assigning a role

81   for *TMEM98* in nanophthalmos has been raised by findings in another study where different

82   heterozygous missense mutations in *TMEM98* were found in patients with high myopia and

83   cone-rod dystrophy [14].

84   Patients with heterozygous or homozygous mutations in the *BEST1* gene can have a range

85   of defects [15]. *BEST1* encodes the bestrophin-1 protein, a transmembrane protein located in

86   the basolateral membrane of the retinal pigment epithelium (RPE) [16]. The predominant

87   disease resulting from heterozygous mutations in *BEST1* is Best vitelliform macular

88   dystrophy, in which subretinal lipofuscin deposits precede vision defects [17]. These patients in

89   early stages have a normal electroretinogram (ERG) but have a defect in electrooculography

90   (EOG) indicative of an abnormality in the RPE. This can progress to retinitis pigmentosa.

91   Five families have been reported with dominant vitreoretinochoroidopathy and

92   nanophthalmos due to three different missense mutations in *BEST1*. Each mutant allele can

93   produce two isoforms, one containing a missense mutation and one containing an in-frame

94   deletion [18]. On the other hand, homozygous null mutations of *BEST1* result in high hyperopia

95   accompanied by abnormal ERGs and EOGs and RPE abnormalities but lacking the

96   vitelliform lesions found in the dominant disease[19]. Similar associations have been seen for

97   mutations in the *CRB1* gene that encodes an apical transmembrane protein important for

98   determining cell polarity in photoreceptors [20]. *CRB1* mutations are most frequently found

99   associated with recessive retinitis pigmentosa or with Leber congenital amaurosis and the

100 disease phenotype observed in patients is very variable suggestive of the influence of

101 genetic modifiers [21, 22]. In addition, hypermetropia and short axial length are a common

102 associations[23]. Furthermore, in two cases, both involving consanguineous families, the

103 retinal dystrophy is associated with nanophthalmos [24, 25].

104

105 Mouse models with mutations in most of these genes have been analysed. Mice which have

106 targeted disruption of the *Best1* gene do not recapitulate the human bestrophinopathy

107 phenotype or have only an enhanced response in EOG (indicative of a defect in the RPE) [26,

108 27]. However, when the common human mutation, W93C, is engineered into the mouse gene,

4

109   both heterozygous and homozygous mice show a distinctive retinal pathology of fluid or

110   debris filled retinal detachments which progress with age [28]. Spontaneous and targeted

111   mutations in mouse *Crb1* have been characterised, and they show similar, though not

112   identical, recessive retinal phenotypes that had variable ages of onset [29-31]. The defects

113   found are focal. Folds appear in the photoreceptor layer that are visualised as white patches

114   on retinal imaging. In a complete loss-of-function allele and the frameshift allele *Crb1^{rd8}* the

115   folds are adjacent to discontinuities in the outer (external) limiting membrane (OLM)

116   accompanied by loss of adherens junctions, and within them the photoreceptors, separated

117   from the RPE, show degeneration [29, 30]. In mice engineered to carry a missense mutation,

118   *Crb1^{C249W}*, that causes retinitis pigmentosa in humans, although the OLM appears intact,

119   retinal degeneration still occurs, albeit later than in the other models [31]. Similar to the human

120   phenotype the extent of the retinal spotting observed in *Crb1* mutants is strongly affected by

121   the genetic background.

122   Two lines of mice with spontaneous mutations in *Mfrp* have been described [32-34]. These do

123   not recapitulate the nanophthalmic phenotype observed in humans. Instead both have the

124   same recessive phenotype of white spots on the retina, which correlate with abnormal cells

125   below the retina that stain with macrophage markers, and progress to photoreceptor

126   degeneration. For the *Mfrp^{rdx}* mutation, atrophy of the RPE was reported [33] and for *Mfrp^{rd6}* a

127   modest ocular axial length reduction from about 2.87 to 2.83 mm was reported although

128   apparently not statistically significant [35]. A screen for mice with increased intraocular

129   pressure (IOP) found a splice mutation in the *Prss56* gene predicted to produce a truncated

130   protein [8]. The increased IOP was associated with a narrow or closed iridocorneal angle,

131   analogous to that seen in human angle closure glaucoma. In addition these mice have eyes

132   that are smaller than littermates, although the size reduction is variable and slight, ranging

133   from 0 to 10% decrease in axial length. Reduction in axial length only becomes statistically

134   significant after post-natal day seven. More recently it has been shown that mice deficient

135   for *Prss56* have eyes with a decreased axial length and hyperopia [36].

136   In summary the human nanophthalmos mutations modelled in mice produce either a much

137   less severe, or non-significant, axial length reduction (*Prss56*, *Mfrp*) or no effect on eye size

138   (*Best1*, *Crb1*). There are differences in the development of human and mouse eyes which

139   probably underlies the differences in mutant phenotype.

140   To date no mouse models of *TMEM98* have been reported. We describe here

141   characterisation of a mouse mutation in *Tmem98*, which results in a dominant phenotype of

5

142   retinal folds. In addition we engineer the two human nanophthalmos-associated missense

143   mutations of *TMEM98* into the mouse gene and show that these mice also, when

144   homozygous or when compound heterozygous, have the same retinal fold phenotype but do

145   not have a statistically significant reduction in eye size.

146

MATERIALS AND METHODS

Mice

149   All mouse work was carried out in compliance with UK Home Office regulations under a UK

150   Home Office project licence and experiments adhered to the ARVO Statement for the Use of

151   Animals in Ophthalmic and Vision Research. Clinical examinations were performed as

152   previously described [37]. Fundus imaging was carried out as described [38]. Mice carrying a

153   targeted knockout-first conditional-ready allele of *Tmem98, Tmem98*[tm1a(EUCOMM)Wtsi] (hereafter

154   *Tmem98*[tm1a]), were obtained from the Sanger Institute [39]. *Tmem98*[tm1a/+] mice were crossed

155   with mice expressing Cre in the germ-line to convert this 'knockout-first' allele to the reporter

156   knock-out allele *Tmem98*[tm1b(EUCOMM)Wtsi] (hereafter *Tmem98*[tm1b]). In this allele the DNA

157   between the loxP sites in the targeting cassette which includes the neo selection gene and

158   the critical exon 4 of *Tmem98* is deleted. To create the *Tmem98*[H196P] allele the CRISPR

159   design site http://www.crispr.mit.edu was used to design guides and the selected guide

160   oligos ex7_Guide1 and ex7_Guide2 (Supplementary Table S1) were annealed and cloned

161   into the *Bbs I* site of the SpCas9 and chimeric guide RNA expression plasmid px330 [40]

162   (pX330-U6-Chimeric_BB-CBh-hSpCas9 was a gift from Feng Zhang (Addgene plasmid

163   #42230, https://www.addgene.org/)). Following pronuclear injection of this plasmid along

164   with repair oligo H196P (Supplementary Table S1) the injected eggs were cultured overnight

165   to the 2-cell stage and transferred into pseudopregnant females. To create the *Tmem98*[A193P]

166   allele Edit-R crRNA (sequence 5'- CCAAUCACUGUCUGCCGCUG-3') (Dharmacon) was

167   annealed to tracrRNA (Sigma) in IDT Duplex buffer (IDT). This, along with Geneart Platinum

168   Cas9 nuclease (Invitrogen B25641) and repair oligo A193P (Supplementary Table S1) were

169   used for pronuclear injection as described above. Pups born were screened for the targeted

170   changes by sequencing PCR fragments generated using the oligos ex7F and ex7R

171   (Supplementary Table S2) and lines established carrying the targeted missense mutations.

172   Genotyping was initially done by PCR, and sequencing where appropriate, using the primers

173   in Supplementary Table S2. Subsequently most genotyping was performed by Transnetyx

174   using custom designed assays (http://www.transnetyx.com). All lines were maintained on the

175   C57BL/6J mouse strain background.

176

DNA Sequencing

178   The candidate interval was captured using a custom Nimblegen array and sequenced with

179   454 technology by Edinburgh Genomics (formerly known as GenePool)

180   (http://www.genomics.ed.ac.uk).

181

Bioinformatics

183   Multiple protein sequence alignments were generated with the program Clustal Omega[41].

184   The possible impact of missense mutations on protein structure and function was evaluated

185   using Polyphen-2 (http://genetics.bwh.harvard.edu/pph2/)[42]. HMM-HMM comparison was

186   used for protein homology detection[43]. For protein structure prediction Phyre2 was used

187   (http://www.sbg.bio.ic.ac.uk/phyre2/)[44]. We used PyMOL for protein structure visualization[45].

188   SCWRL[46] and the FoldX web server[47] were used to evaluate the effect of amino acid

189   substitutions on protein stability.

190

Electroretinography

192   Prior to electroretinography mice were dark adapted overnight (>16 hours) and experiments

193   were carried out in a darkened room under red light using an HMsERG system

194   (Ocuscience). Mice were anesthetised using isofluorane and their pupils dilated by the

195   topical application of 1% w/v tropicamide. Three grounding electrodes were placed

196   subcutaneously (tail, and each cheek) and silver embedded electrodes were positioned on

197   the corneas using hypromellose eye drops (2.5% methylcellulose coupling agent) held in

198   place with a contact lens. Animals were kept on a heated platform to maintain them at 37°C

199   and monitored using a rectal thermometer. A modified QuickRetCheck (Ocuscience)

200   protocol was used for obtaining full-field scotopic ERGs. Briefly, 4 flashes at 10 mcd.s/m^2 at

201   2 s intervals were followed by 4 flashes at 3 cd.s/m^2 (at 10 s intervals) and then 4 flashes at

202   10 cd.s/m^2 (at 10 s intervals).

203

Histology and Immunostaining

Mice were culled, eyes enucleated and placed into Davidson's fixative (28.5% ethanol, 2.2% neutral buffered formalin, 11% glacial acetic acid) for 1 hour (cryosectioning) or overnight (wax embedding) except for the eye used for Fig. 1 which was placed in 10% neutral buffered formalin for 24 hours before immersion in Davidson's fixative. Prior to wax embedding eyes were dehydrated through an ethanol series. Haematoxylin and eosin staining was performed on 5 or 10 µm paraffin embedded tissue sections and images captured using a Nanozoomer XR scanner (Hamamatsu) and viewed using NDP.view2 software. For cryosectioning, fixed eyes were transferred to 5% sucrose in PBS and once sunk transferred to 20% sucrose in PBS overnight. Eyes were then embedded in OCT compound and cryosectioned at 14 µM. For immunostaining on cryosections, slides were washed with water then PBS and post-fixed in acetone at -20°C for 10 minutes. They were then rinsed with water, blocked in 10% donkey serum (DS), 0.1% Tween-20 in TBS (TBST) for one hour and then incubated with primary antibodies diluted in TBST with 5% DS for two hours at room temperature or overnight at 4°C. Subsequently, after washing with TBST, the slides were incubated with Alexa Fluor secondary antibodies (Invitrogen) diluted 1:400 in TBST with 5% DS at room temperature for one hour. Following washing with TBST coverslips were mounted on slides in Prolong Gold (ThermoFisher Scientific) and confocal images acquired on a Nikon A1R microscope. Images were processed using either NIS-Elements or ImageJ software.

Eye size measurment

Eyes from male mice were enucleated and kept in PBS prior to measuring to prevent drying out. The analysis was restricted to males as significant differences in axial length have been reported in the C57BL/6 strain between male and female mice[48]. Axial length measurements were made from the base of the optic nerve to the centre of the cornea using a Mitutoyo Digital ABS Caliper 6"/150mm, item number: 500-196-20.

Antibodies

Primary antibodies used are listed in Table 1. DNA was stained with TOTO-3 (Invitrogen) or 4',6-Diamidine-2'-phenylindole dihydrochloride (DAPI).

8

235

Transmission Electron Microscopy

237 Samples were fixed in 2% EM grade glutaraldehyde (TAAB Laboratory Equipment,
238 Aldermaston, UK) in sodium cacodylate buffer at 4°C overnight, post-fixed in 1% osmium
239 tetroxide (Agar Scientific , Essex, UK), dehydrated in increasing concentrations of acetone
240 and impregnated with increasing concentrations of epoxy resin (TAAB Laboratory
241 Equipment). Embedding was carried out in 100% resin at 60°C for 24 hours. Semi-thin
242 survey sections of 1 µm, stained with toluidine blue, were taken to determine relevant area.
243 Ultrathin sections (approximately 70 nm) were then cut using a diamond knife on a Leica EM
244 UC7 ultramicrotome (Leica, Allendale, NJ, USA). The sections were stretched with
245 chloroform to eliminate compression and mounted on Pioloform-filmed copper grids (Gilder
246 Grids, Grantham UK). To increase contrast the grids were stained with 2% aqueous uranyl
247 acetate and lead citrate (Leica). The grids were examined using a Philips CM 100
248 Compustage (FEI) Transmission Electron Microscope. Digital images were collected using
249 an AMT CCD camera (Deben UK Ltd., Suffolk, UK).

250

Statistics

252 For the data shown in Figures 1, 2,3 and Supplementary Figure S7 the graphs were created
253 and unpaired t tests with Welch's correction were performed using the program Graphpad
254 Prism. For the data shown in Tables 2, S3 and S4 chi square tests were performed using
255 http://graphpad.com/quickcalcs. A value of P<0.05 was considered significant.

256

257 # RESULTS

258 ***Rwhs* is a missense mutation of the *Tmem98* gene**

259 The *N*-ethyl-*N*-nitrosourea (ENU)-induced mouse mutation retinal white spots (*Rwhs*) was
260 found in a screen for dominant eye mutations [37]. Mice heterozygous for the mutation have
261 white patches on retinal imaging, apparently corresponding to folds or invaginations of the
262 photoreceptor layers (Fig. 1A-B). Initial mapping indicated that *Rwhs* was located within an
263 8.5 Mb region of chromosome 11 [37]. The retinal phenotype was found on a mixed Balb/c and
264 C3H background. When *Rwhs* mutant mice were backcrossed to the C57BL/6J strain to
265 refine the genetic mapping, some obligate heterozygous mice had retinas with a normal

266   appearance, indicating that the dominant *Rwhs* phenotype is not completely penetrant and

267   that modifiers in the C57BL/6J strain can attenuate it (Supplementary Fig. S1A-D). Crossing

268   *Rwhs* to the wild-derived *CAST* strain to introduce a different and diverse genetic

269   background, restored the retinal phenotype (Supplementary Fig. S1E-F). Intercrossing of

270   heterozygous mice produced no homozygous offspring at weaning, whereas at late

271   gestation (E17.5-E18.5) fetuses of the three expected genotypes were present at Mendelian

272   ratios indicating that homozygous *Rwhs* is perinatally lethal (Table 2) (an initial report

273   suggesting that homozygous *Rwhs* mice were viable was incorrect and due to mapping

274   errors [37]). We mapped this lethal phenotype by intercrossing recombinant animals and

275   refined the critical interval to a 200 kb region between the single nucleotide polymorphism

276   markers rs216663786 and rs28213460 on chromosome 11. This region contains the

277   *Tmem98* gene and parts of the *Myo1d* and *Spaca3* genes. We amplified and sequenced all

278   the exons and flanking regions from this region from *Rwhs* mutant mice along with controls.

279   In addition we captured and sequenced all genomic DNA in the candidate interval. We found

280   only a single nucleotide change in the mutant strain compared to the strain of origin, a T to C

281   transition, in exon 5 of *Tmem98* (position 11:80,817,609 Mouse Dec. 2011 (GRCm38/mm10)

282   Assembly (https://genome.ucsc.edu/)) (Fig. 1C). This mutation leads to the substitution of

283   the non-polar aliphatic amino acid, isoleucine, by the polar amino acid threonine (I135T,

284   numbering from entry Q91X86, http://www.uniprot.org). This amino acid substitution is

285   predicted to be possibly damaging by the polymorphism prediction tool PolyPhen-2[42].

286   TMEM98 is a 226 amino acid protein annotated with a transmembrane domain spanning

287   amino acids 4-24 close to the N-terminus (http://www.uniprot.org). It is highly conserved

288   across species; mouse and human TMEM98 share 98.7% amino acid identity and between

289   mouse and *Ciona intestinalis*, the closest invertebrate species to the vertebrates, there is

290   38.6% amino acid identity in which I135 is conserved (Supplementary Fig. S2). TMEM98 has

291   been reported to be a single-pass type II transmembrane protein in which the C-terminal part

292   is extracellular [49]. *TMEM98* is widely expressed and is reported to be most highly expressed

293   in human and mouse RPE (http://www.biogps.org). We confirmed its high expression in the

294   RPE and, within the retina, we also find expression at a lower level in the ganglion cell layer

295   (Fig. 1D). To assess retinal function electroretinography was carried out on *Tmem98^{I135T/+}*

296   and wild-type mice (Fig. 1E and F). There were no significant differences in the a-wave or b-

297   wave amplitudes between the *Tmem98^{I135T/+}* and wild-type mice.

298   We also investigated the effect of loss-of-function of *Tmem98*. Heterozygous loss-of-function

299   mice are viable and fertile and have normal retinas (Supplementary Fig. S6D and F).

10

300 Matings of heterozygous mice carrying the "knock-out first" *Tmem98^tm1a* allele produced no

301 homozygous offspring (Supplementary Table S3) demonstrating that loss-of-function of

302 *Tmem98* is lethal. At E16.5-E17.5 the three expected genotypes were present at Mendelian

303 ratios (Supplementary Table S3) and in one litter collected at birth there were three

304 homozgyotes and three wild-types indicating that lethality occurs between birth and weaning.

305

The Human Nanophthalmos Missense Mutations Cause a Retinal Phenotype in the

307 **Mouse**

308 Three mutations in *TMEM98* have been implicated in autosomal dominant nanophthalmos in

309 human families [12, 13]. Two are missense mutations, A193P and H196P. Both missense

310 mutations affect amino acids that are highly conserved (Supplementary Fig. S2) Both are

311 predicted to be probably damaging by the polymorphism prediction tool PolyPhen-2[42].

312 To investigate the effect of the two missense mutations we used CRISPR-Cas9 to introduce

313 A193P and H196P into the mouse gene and established lines carrying each. Western blot

314 analysis using a validated anti-TMEM98 antibody (Supplementary Fig. S3A) showed that the

315 mutant proteins are expressed (Supplementary Fig. S3B). Heterozygous mice for both

316 missense mutations were viable and fertile and did not exhibit any gross eye or retinal

317 defects when examined between 5-9 months of age (Supplementary Fig. S4, *Tmem98^A193P/+*,

318 n=10; *Tmem98^H196P/+*, n=19). In contrast to the *Tmem98^I135T* and knock-out alleles,

319 homozygotes for both the *Tmem98^A193P* and *Tmem98^H196P* alleles were viable and found at

320 the expected Mendelian ratios (Supplementary Table S4). The eyes of homozygous mice do

321 not appear to be significantly different in axial length when compared to wild-type eyes (Fig.

322 2A). Although the mean length of homozygous *Tmem98^H196P* eyes is ~7% smaller than

323 controls this does not have statistical support (P=0.1). From about 3 months of age we found

324 that white patches developed on the retinas of the homozygous mice and on histological

325 examination we found folds or invaginations in the retinal layers (Fig. 2B). The appearance

326 of the white patches was progressive; at younger ages the retinas of some homozygous

327 mice appeared normal with patches becoming apparent as they aged (Supplementary Fig.

328 S5). In the A193P line only 6 of 7 homozygotes were found to have retinal defects at 6

329 months of age; the seventh developed white patches on the retina by 9 months. In the

330 H196P line 4/20 homozygous mice that were examined between 3 and 3.5 months of age

331 appeared to have normal retinas. We crossed the lines together to generate compound

332 heterozygotes. All *Tmem98^A193P/H196P* (n=4), *Tmem98^I135T/ A193P* (n=7) and *Tmem98^I135T/H196P*

11

333   (n=5) mice examined also displayed a similar phenotype of white patches on the retina (Fig.

334   2B and data not shown). We also crossed $Tmem98^{H196P}$ mice with mice carrying a loss-of-

335   function allele $Tmem98^{tm1b}$. Compound heterozygous mice were viable and of 17 mice

336   examined all had normal retinas except for one mouse which had three faint spots on one

337   retina at one year of age (Supplementary Fig. S6). These results suggest that a threshold

338   level of the mutant missense TMEM98^{H196P} and TMEM98^{A193P} proteins is required to elicit the

339   formation of white patches on the retina and that the missense mutations found in the human

340   nanophthalmos patients are not loss-of-function. Furthermore, mice heterozygous for

341    $Tmem98^{tm1b}$ with a wild type allele do not have the retinal phenotype (Supplementary Fig.

342   S6).

343   To assess retinal function electroretinography was carried out on

344    $Tmem98^{A193P/A193P}$,$Tmem98^{H196P/H196P}$ and control mice (Fig. 3). There were no significant

345   differences in the a-wave or b-wave amplitudes between the control and the mutant mice. To

346   determine if there was any deterioration in retinal function in older mice we also tested

347    $Tmem98^{H196P/H196P}$and control mice at 9-11 months of age but again we did not find any

348   significant differences in the a-wave or b-wave amplitutes between the control and the

349   mutant mice (Supplementary Fig. S7).

350   **Characterisation of the Retinal Folds Caused by the A193P and H196P Mutations**

351   We investigated the retinal folds by immunostaining of retinal sections. We found that in the

352   interior of retinal folds the outer segment layer is massively expanded as demonstrated by

353   positive staining for the transmembrane protein prominin-1 and the rod and cone opsins

354   (rhodopsin and ML opsin), indicating that the folds are filled with excess, disorganised outer

355   segments or remnants of outer segments (Fig. 4).

356   The retinal folds seen in other mutant mouse lines are accompanied by defects in the OLM.

357   This structure is formed by adherens junctions between the Müller glia cells and the

358   photoreceptors. We investigated the integrity of the OLM in our mutant mice by staining for

359   β-catenin (Fig. 5A-D). In control mice and in the regions of the retinas of mutant mice

360   unaffected by folds the OLM appeared intact. However, at the folds the OLM is clearly

361   disrupted and gaps can be seen suggesting that cell-cell connections have been broken.

362   Reactive gliosis indicated by upregulation of GFAP in the Müller cells is a response to retinal

363   stress, injury or damage [50]. We observed abnormal GFAP staining in the mutant retinas that

364   was confined to the regions with folds, indicating that in these areas, but not elsewhere in

365   the retina, there is a stress response (Fig. 5E-H, Supplementary Fig. S8A-D). We also

12

366 stained for F4/80, a marker for macrophages/microglia. In the mutant retinas positive

367 staining was found in the interior of retinal folds but not elsewhere in the photoreceptor layer

368 (Fig. 5J-L, Supplementary Fig. S8F-H). The amoeboid shape of the positively-stained cells

369 suggests that they are macrophages that have infiltrated into the retinal folds containing

370 excess and disorganised outer segments and that they are phagocytosing degenerating

371 outer segments. We did not observe melanin within the macrophages indicating that they

372 had not engulfed pigmented RPE cells. Finally, we examined by transmission electron

373 microscopy the ultrastructural architecture of the boundary between the RPE and outer

374 segments (Fig. 6). For the homozygous mutants, in retinal areas without folds, the boundary

375 between outer segments and RPE appeared normal (compare Fig. 6A with Fig. 6B and D).

376 However, in the areas with folds the outer segments were disorganised and appeared to be

377 degenerating, with cavitites and other celluar debris apparent (Fig. 6C and 6E).

378

DISCUSSION

Rwhs is Caused by a Missense Mutation in *Tmem98* that is Homozygous Lethal

381 Here we report that the ENU-induced dominant retinal white spotting phenotype, *Rwhs*, is

382 caused by an I135T missense mutation in the highly conserved transmembrane protein

383 encoding gene *Tmem98*. We also found that when homozygous the *Tmem98^{I135T}* allele is

384 perinatally lethal. *Tmem98* was one of the genes included in an international project to

385 produce and phenotype knockout mouse lines for 20,000 genes [51]. The targeted allele,

386 *Tmem98^{tm1a}*, was subjected to a high-content phenotyping pipeline (results available at

387 http://www.mousephenotype.org/data/genes/MGI:1923457). It was found to be lethal pre-

388 weaning as homozygotes, but no significant heterozygous phenotypic variation from wild-

389 type was reported. Neither their slit lamp analysis nor our retinal examination found any eye

390 defects in knock-out heterozygous mice (Supplementary Fig. S6D and F). We also found

391 that *Tmem98^{tm1a}* is homozygous lethal and narrowed the stage of lethality to the perinatal

392 stage (Supplementary Table S2). This suggests that haploinsufficency for TMEM98 protein

393 does not cause a retinal phenotype and that the I135T mutation in TMEM98 is not a loss-of-

394 function allele but changes the protein's function leading to the retinal white spotting

395 phenotype.

Phenotype of Human Nanophthalmos Associated *TMEM98* Missense Mutations in the Mouse

398 *Tmem98* has been previously suggested to be a novel chemoresistance-conferring gene in

399 hepatoceullular carcinoma [52]. It has also been reported to be able to promote the

400 differentiation of T helper 1 cells and to be involved in the invasion and migration of lung

401 cancer cells [49, 53]. Recently it has been reported that TMEM98 interacts with MYRF and

402 prevents its autocatalytic cleavage [54]. In relation to human disease two TMEM98 missense

403 mutations, A193P and H196P, have been reported to be associated with dominant

404 nanophthalmos [12, 13]. We introduced these mutations into the mouse gene and found that

405 mice homozygous for either, or compound heterozygous for both, developed white patches

406 on their retinas accompanied by retinal folds, replicating the dominant phenotype found in

407 the ENU-induced allele. We also observed for all three alleles separation of the RPE away

408 from the neural retina in the areas under the folds. Mice lacking *Tmem98* do not survive after

409 birth (Supplementary Table S3). The three missense mutations described here are not null.

410 The two human-equivalent mutations in the mouse are homozygous viable (Supplementary

411 Table S4), and the mouse mutation, when in combination with a knock-out allele is also

412 viable (data not shown). Furthermore, the H196P missense mutation in combination with a

413 gene knockout has no detectable eye phenotype and the mice are viable (Supplementary

414 Fig. S6). This indicates that the recessive mutations are not loss of function, but are gain of

415 function with, in the case of H196P at least, a threshold dosage requirement. However, the

416 phenotypes are different from the reported dominant nanophthalmos caused by the same

417 mutations in humans.

418 Other genes causing nanophthalmos may also be gain of function. The serine protease

419 *PRSS56* is a recessive posterior microphthamia or nanophthalmos mutant gene in humans,

420 with both identified mutations affecting the C-terminus of the protein [8]. The mouse mutant

421 model of this gene, which produces a variable and slight reduction in ocular length, is a

422 splice site mutation resulting in a truncated protein which nevertheless has normal protease

423 activity *in vitro* [8]. Recently the phenotype of a null allele of *Prss56* has been described and it

424 does cause some reduction in ocular size and hyperopia [36].

425 The mouse model of the nanophthalmos gene, *Mfrp*, does not reproduce the human

426 phenotype. Rather, loss of function of this gene results in white spots apparent on retinal

427 imaging (retinitis punctata albicans) but these have different origin from the phenotype we

428 observe, and progress to photoreceptor degeneration. It has been reported that the *Mfrp*

429 knockout mice have eyes that are slightly (but not statistically significantly) smaller, by about

430 2% in axial length[35]. Our analysis of the human-equivalent mouse *Tmem98* mutations show

431 that that neither have statistically significant size reductions, although the H196P line is ~7%

14

432   shorter It is worth noting that different strains of mice have measurably different ocular size.

433   Strain differences of up to 2% and sex differences of over 1.5% have been reported[48].

434   Two genes that are infrequently associated with nanopthalmos, *CRB1* and *BEST1*, both can

435   produce a mouse phenotype apparently indistinguishable from the one we describe here.

436   Furthermore, the knockout mouse model of the nuclear receptor gene, *Nrl*, also develops

437   retinal folds during post-natal life[55]. The *Nrl* mutant eye has defects in the outer limiting

438   membrane (OLM), a component of which is the CRB1 protein. The *Tmem98* mutations have

439   OLM defects, but we cannot ascertain whether these defects are the primary cause of the

440   folds or a secondary consequence.

441   Retinal folds are a characteristic of nanophthalmic eyes and this is usually attributed to a

442   differential growth of neural retina within the smaller optic cup. Our data show that folds can

443   be seen in a normal-sized eye, but we do not know whether there is nevertheless excess

444   growth of the neural retina. The retinal defects we see are not associated with an ERG

445   deficit, suggesting that the rest of the retina, unaffected by the folds, is functionally normal.

446   Notable is the detachment of the retina from the RPE within the folds . In the *Nrl* and *Crb1*

447   mutant eyes the photoreceptors that have lost their connection to the RPE can be seen to

448   degenerate. We see no evidence of photoreceptor degeneration in the *Tmem98* mutants.

449   The mechanism of the pathology is still unclear. As *Tmem98* is strongly expressed in the

450   RPE, and not at all in the photoreceptors, it is likely that RPE is the affected tissue. The key

451   observation in these and other mouse models of nanophthalmos is that the defects are focal

452   and progressive, suggesting that secondary events exacerbate an underlying but (given

453   ERG data) non-pathological defect. The accumulation of photoreceptor cell debris below the

454   retinal folds suggests a focal defect in outer segment phagocytosis but one that does not

455   lead to photoreceptor degeneration. Three of the genes associated with nanophthalmos are

456   expressed in the RPE; *Tmem98*, *Best1* and *Mfrp*. *Crb1* is expressed in photoreceptors and

457   *Prss56*, a secreted serine protease, is expressed in the Müller cells. It is possible that these

458   genes interact and affect a common pathway, indeed upregulation of *Prss56* has been

459   observed in *Mfrp* mutants [56].

460

Effect on TMEM98 Protein Structure of the Missense Mutations

462   TMEM98 has structural homology to Cyclin-D1-binding protein 1 (CCNDBP1) and contains a

463   Grap2 and cyclin-D-interacting (GCIP) domain (pfam13324) spanning amino acids 49-152.

15

464 Based upon the crystal structure of CCNDBP1 following the N-terminal transmembrane

465 domain TMEM98 is predicted to have a five helix bundle structure using PHYRE2[44] (Fig.

466 7A). I135 is located in the third α-helix completely buried within a sterically close-packed

467 hydrophobic core of the domain where it has hydrophobic interactions with amino acids from

468 four of the α-helices (Fig. 7B). SCWRL[46] and FoldX[47] stability calculations indicate that the

469 *Rwhs* mutation T135 is only very mildly destabilising in this homology model. Its side-chain

470 does not show steric clashes with other neighbouring atoms and its buried hydroxyl group

471 forms a favourable hydrogen bond with the main-chain oxygen atom of A132. The stability

472 energy calculation on the mutant TMEM98 domain structure (mean ΔΔG) is 0.28 kcal/mol

473 (>1.6 kcal/mol is considered destabilising). The genetic evidence shows that the I135T is not

474 loss-of-function. The detrimential effect of a mutation leading to loss of thermodynamic

475 stability can be compensated for by the creation of novel functions[57]. This might be the case

476 with the I135T mutation. The two missense mutations that are associated with

477 nanophthalmos introduce a proline in the middle of the final α-helix of the protein which

478 would likely lead to disruption of the secondary structure of the protein[58]. The recent finding

479 that TMEM98 binds to and prevents the self-cleavage of the oligodendrocyte transcription

480 factor MYRF[54] (also highly expressed in the RPE; http://www.biogps.org) will perhaps lead to

481 a mechanistic explanation, although the part of TMEM98 that binds to MYRF was mapped to

482 the N-terminal 88 amino acids and a region between 55-152 amino acids was shown to be

483 required for the cleavage inhibition. As the nanophthalmos patient-specific missense

484 mutations are more C-terminal their effect on this reported interaction will be the subject of

485 future work.

486

Acknowledgements

References

493 1.   Verma AS, FitzPatrick DR. Anophthalmia and microphthalmia. *Orphanet journal of rare
494 diseases* 2007;2:47.
495 2.   Carricondo PC, Andrade T, Prasov L, Ayres BM, Moroi SE. Nanophthalmos: A Review of the
496 Clinical Spectrum and Genetics. *Journal of ophthalmology* 2018;2018.

497   3.   Sundin OH, Leppert GS, Silva ED, et al. Extreme hyperopia is the result of null mutations in
498   MFRP, which encodes a Frizzled-related protein. *Proceedings of the National Academy of Sciences*
499   2005;102:9553-9558.
500   4.   Ayala-Ramirez R, Graue-Wiechers F, Robredo V, Amato-Almanza M, Horta-Diez I, Zenteno JC.
501   A new autosomal recessive syndrome consisting of posterior microphthalmos, retinitis pigmentosa,
502   foveoschisis, and optic disc drusen is caused by a MFRP gene mutation. *Molecular vision*
503   2006;12:1483-1489.
504   5.   Zenteno JC, Buentello-Volante B, Quiroz-González MA, Quiroz-Reyes MA. Compound
505   heterozygosity for a novel and a recurrent MFRP gene mutation in a family with the nanophthalmos-
506   retinitis pigmentosa complex. *Molecular vision* 2009;15:1794.
507   6.   Neri A, Leaci R, Zenteno JC, Casubolo C, Delfini E, Macaluso C. Membrane frizzled-related
508   protein gene–related ophthalmological syndrome: 30-month follow-up of a sporadic case and review
509   of genotype-phenotype correlation in the literature. *Molecular vision* 2012;18:2623.
510   7.   Gal A, Rau I, El Matri L, et al. Autosomal-recessive posterior microphthalmos is caused by
511   mutations in PRSS56, a gene encoding a trypsin-like serine protease. *The American Journal of Human*
512   *Genetics* 2011;88:382-390.
513   8.   Nair KS, Hmani-Aifa M, Ali Z, et al. Alteration of the serine protease PRSS56 causes angle-
514   closure glaucoma in mice and posterior microphthalmia in humans and mice. *Nature Genetics*
515   2011;43:579.
516   9.   Orr A, Dubé M-P, Zenteno JC, et al. Mutations in a novel serine protease PRSS56 in families
517   with nanophthalmos. *Molecular vision* 2011;17:1850.
518   10.   Kiefer AK, Tung JY, Do CB, et al. Genome-wide analysis points to roles for extracellular matrix
519   remodeling, the visual cycle, and neuronal development in myopia. *PLoS genetics* 2013;9:e1003299.
520   11.   Verhoeven VJ, Hysi PG, Wojciechowski R, et al. Genome-wide meta-analyses of
521   multiancestry cohorts identify multiple new susceptibility loci for refractive error and myopia. *Nat*
522   *Genet* 2013;45:314-318.
523   12.   Awadalla MS, Burdon KP, Souzeau E, et al. Mutation in TMEM98 in a large white kindred
524   with autosomal dominant nanophthalmos linked to 17p12-q12. *JAMA ophthalmology* 2014;132:970-
525   977.
526   13.   Khorram D, Choi M, Roos BR, et al. Novel TMEM98 mutations in pedigrees with autosomal
527   dominant nanophthalmos. *Molecular vision* 2015;21:1017-1023.
528   14.   Sun W, Zhang Q. Does the association between TMEM98 and nanophthalmos require
529   further confirmation? *JAMA ophthalmology* 2015;133:358-359.
530   15.   Boon CJ, Klevering BJ, Leroy BP, Hoyng CB, Keunen JE, den Hollander AI. The spectrum of
531   ocular phenotypes caused by mutations in the BEST1 gene. *Progress in retinal and eye research*
532   2009;28:187-205.
533   16.   Marmorstein AD, Marmorstein LY, Rayborn M, Wang X, Hollyfield JG, Petrukhin K.
534   Bestrophin, the product of the Best vitelliform macular dystrophy gene (VMD2), localizes to the
535   basolateral plasma membrane of the retinal pigment epithelium. *Proceedings of the National*
536   *Academy of Sciences* 2000;97:12758-12763.
537   17.   Petrukhin K, Koisti MJ, Bakall B, et al. Identification of the gene responsible for Best macular
538   dystrophy. *Nature genetics* 1998;19:241.
539   18.   Yardley J, Leroy BP, Hart-Holden N, et al. Mutations of VMD2 splicing regulators cause
540   nanophthalmos and autosomal dominant vitreoretinochoroidopathy (ADVIRC). *Investigative*
541   *ophthalmology & visual science* 2004;45:3683-3689.
542   19.   Burgess R, Millar ID, Leroy BP, et al. Biallelic mutation of BEST1 causes a distinct retinopathy
543   in humans. *American journal of human genetics* 2008;82:19-31.
544   20.   Pellikka M, Tanentzapf G, Pinto M, et al. Crumbs, the Drosophila homologue of human
545   CRB1/RP12, is essential for photoreceptor morphogenesis. *Nature* 2002;416:143.

546   21.   den Hollander AI, Jacoline B, de Kok YJ, et al. Mutations in a human homologue of
547   Drosophila crumbs cause retinitis pigmentosa (RP12). *Nature genetics* 1999;23:217.
548   22.   den Hollander AI, Heckenlively JR, van den Born LI, et al. Leber congenital amaurosis and
549   retinitis pigmentosa with Coats-like exudative vasculopathy are associated with mutations in the
550   crumbs homologue 1 (CRB1) gene. *The American Journal of Human Genetics* 2001;69:198-203.
551   23.   Henderson RH, Mackay DS, Li Z, et al. Phenotypic variability in patients with retinal
552   dystrophies due to mutations in CRB1. *The British journal of ophthalmology* 2011;95:811-817.
553   24.   Zenteno JC, Buentello-Volante B, Ayala-Ramirez R, Villanueva-Mendoza C. Homozygosity
554   mapping identifies the Crumbs homologue 1 (Crb1) gene as responsible for a recessive syndrome of
555   retinitis pigmentosa and nanophthalmos. *American Journal of Medical Genetics Part A*
556   2011;155:1001-1006.
557   25.   Paun CC, Pijl BJ, Siemiatkowska AM, et al. A novel crumbs homolog 1 mutation in a family
558   with retinitis pigmentosa, nanophthalmos, and optic disc drusen. *Molecular vision* 2012;18:2447.
559   26.   Marmorstein LY, Wu J, McLaughlin P, et al. The light peak of the electroretinogram is
560   dependent on voltage-gated calcium channels and antagonized by bestrophin (best-1). *The Journal*
561   *of general physiology* 2006;127:577-589.
562   27.   Milenkovic A, Brandl C, Milenkovic VM, et al. Bestrophin 1 is indispensable for volume
563   regulation in human retinal pigment epithelium cells. *Proceedings of the National Academy of*
564   *Sciences* 2015;112:E2630-E2639.
565   28.   Zhang Y, Stanton JB, Wu J, et al. Suppression of Ca 2+ signaling in a mouse model of Best
566   disease. *Human molecular genetics* 2010;19:1108-1118.
567   29.   Mehalow AK, Kameya S, Smith RS, et al. CRB1 is essential for external limiting membrane
568   integrity and photoreceptor morphogenesis in the mammalian retina. *Human molecular genetics*
569   2003;12:2179-2189.
570   30.   van de Pavert SA, Kantardzhieva A, Malysheva A, et al. Crumbs homologue 1 is required for
571   maintenance of photoreceptor cell polarization and adhesion during light exposure. *Journal of Cell*
572   *Science* 2004;117:4169-4177.
573   31.   van de Pavert SA, Meuleman J, Malysheva A, et al. A single amino acid substitution
574   (Cys249Trp) in Crb1 causes retinal degeneration and deregulates expression of pituitary tumor
575   transforming gene Pttg1. *Journal of Neuroscience* 2007;27:564-573.
576   32.   Kameya S, Hawes NL, Chang B, Heckenlively JR, Naggert JK, Nishina PM. Mfrp, a gene
577   encoding a frizzled related protein, is mutated in the mouse retinal degeneration 6. *Human*
578   *molecular genetics* 2002;11:1879-1886.
579   33.   Fogerty J, Besharse JC. 174delG mutation in mouse MFRP causes photoreceptor
580   degeneration and RPE atrophy. *Investigative ophthalmology & visual science* 2011;52:7256-7266.
581   34.   Hawes NL, Chang B, Hageman GS, et al. Retinal degeneration 6 (rd6): a new mouse model for
582   human retinitis punctata albescens. *Investigative ophthalmology & visual science* 2000;41:3149-
583   3157.
584   35.   Velez G, Tsang SH, Tsai Y-T, et al. Gene Therapy Restores Mfrp and Corrects Axial Eye Length.
585   *Scientific Reports* 2017;7:16151.
586   36.   Paylakhi S, Labelle-Dumais C, Tolman NG, et al. Muller glia-derived PRSS56 is required to
587   sustain ocular axial growth and prevent refractive error. *PLoS Genet* 2018;14:e1007244.
588   37.   Thaung C, West K, Clark BJ, et al. Novel ENU-induced eye mutations in the mouse: models
589   for human eye disease. *Human molecular genetics* 2002;11:755-767.
590   38.   White JK, Gerdin A-K, Karp NA, et al. Genome-wide generation and systematic phenotyping
591   of knockout mice reveals new roles for many genes. *Cell* 2013;154:452-464.
592   39.   Skarnes WC, Rosen B, West AP, et al. A conditional knockout resource for the genome-wide
593   study of mouse gene function. *Nature* 2011;474:337.

594   40.   Cong L, Ran FA, Cox D, et al. Multiplex genome engineering using CRISPR/Cas systems.
595   *Science* 2013;1231143.
596   41.   Sievers F, Wilm A, Dineen D, et al. Fast, scalable generation of high-quality protein multiple
597   sequence alignments using Clustal Omega. *Molecular systems biology* 2011;7:539.
598   42.   Adzhubei IA, Schmidt S, Peshkin L, et al. A method and server for predicting damaging
599   missense mutations. *Nature methods* 2010;7:248-249.
600   43.   Soding J. Protein homology detection by HMM-HMM comparison. *Bioinformatics (Oxford,*
601   *England)* 2005;21:951-960.
602   44.   Kelley LA, Mezulis S, Yates CM, Wass MN, Sternberg MJ. The Phyre2 web portal for protein
603   modeling, prediction and analysis. *Nature protocols* 2015;10:845-858.
604   45.   Janson G, Zhang C, Prado MG, Paiardini A. PyMod 2.0: improvements in protein sequence-
605   structure analysis and homology modeling within PyMOL. *Bioinformatics (Oxford, England)*
606   2017;33:444-446.
607   46.   Wang Q, Canutescu AA, Dunbrack RL, Jr. SCWRL and MolIDE: computer programs for side-
608   chain conformation prediction and homology modeling. *Nature protocols* 2008;3:1832-1847.
609   47.   Schymkowitz J, Borg J, Stricher F, Nys R, Rousseau F, Serrano L. The FoldX web server: an
610   online force field. *Nucleic acids research* 2005;33:W382-388.
611   48.   Puk O, Dalke C, Favor J, de Angelis MH, Graw J. Variations of eye size parameters among
612   different strains of mice. *Mamm Genome* 2006;17:851-857.
613   49.   Fu W, Cheng Y, Zhang Y, et al. The Secreted Form of Transmembrane Protein 98 Promotes
614   the Differentiation of T Helper 1 Cells. *Journal of interferon & cytokine research : the official journal*
615   *of the International Society for Interferon and Cytokine Research* 2015;35:720-733.
616   50.   Lewis GP, Fisher SK. Up-regulation of glial fibrillary acidic protein in response to retinal
617   injury: its potential role in glial remodeling and a comparison to vimentin expression. *International*
618   *review of cytology* 2003;230:264-290.
619   51.   Brown SD, Holmes CC, Mallon A-M, Meehan TF, Smedley D, Wells S. High-throughput mouse
620   phenomics for characterizing mammalian gene function. *Nature Reviews Genetics* 2018;1.
621   52.   Ng KT, Lo CM, Guo DY, et al. Identification of transmembrane protein 98 as a novel
622   chemoresistance-conferring gene in hepatocellular carcinoma. *Molecular cancer therapeutics*
623   2014;13:1285-1297.
624   53.   Mao M, Chen J, Li X, Wu Z. siRNA-TMEM98 inhibits the invasion and migration of lung cancer
625   cells. *International journal of clinical and experimental pathology* 2015;8:15661-15669.
626   54.   Huang H, Teng P, Du J, et al. Interactive repression of MYRF self-cleavage and activity in
627   oligodendrocyte differentiation by TMEM98 protein. *The Journal of neuroscience : the official journal*
628   *of the Society for Neuroscience* 2018.
629   55.   Stuck MW, Conley SM, Naash MI. Defects in the outer limiting membrane are associated
630   with rosette development in the Nrl-/- retina. *PLoS One* 2012;7:e32484.
631   56.   Soundararajan R, Won J, Stearns TM, et al. Gene profiling of postnatal Mfrprd6 mutant eyes
632   reveals differential accumulation of Prss56, visual cycle and phototransduction mRNAs. *PloS one*
633   2014;9:e110299.
634   57.   Tokuriki N, Stricher F, Serrano L, Tawfik DS. How protein stability and new functions trade
635   off. *PLoS computational biology* 2008;4:e1000002.
636   58.   Barlow DJ, Thornton JM. Helix geometry in proteins. *Journal of molecular biology*
637   1988;201:601-619.

638

639   **Table**

640 **Table 1. Primary antibodies**

Antibody	Source	Product No	Concentration used
anti-TMEM98	proteintech	14731-1-AP	1:5000 (WB), 1:100 (IF)
anti-α-Tubulin	Sigma-Aldrich	T5168	1:10,000 (WB)
anti-Prominin 1	proteintech	18470-1-AP	1:100 (IF)
anti-Rhodopsin	Millipore	MAB5356	1:500 (IF)
anti-ML Opsin	Millipore	AB5405	1:500 (IF)
anti-GFAP	abcam	ab7260	1:500 (IF)
anti-β-Catenein	Cell Signaling Technology	19807S	1:500 (IF)
Anti-F4/80	AbD Serotec	MCA497EL	1:500 (IF)

641 Key: WB=Western blotting, IF=immunofluorescence

642

643 **Table 2. *Tmem98$^{Rwhs/+}$* intercross genotyping results**

Age	WT	*Rwhs*/+	*Rwhs/Rwhs*	Total	P*
adult	34	79	0	113	<0.0001
E17.5-E18.5	2	12	5	19	0.3225

644 *Test for significance using chi-square test

20
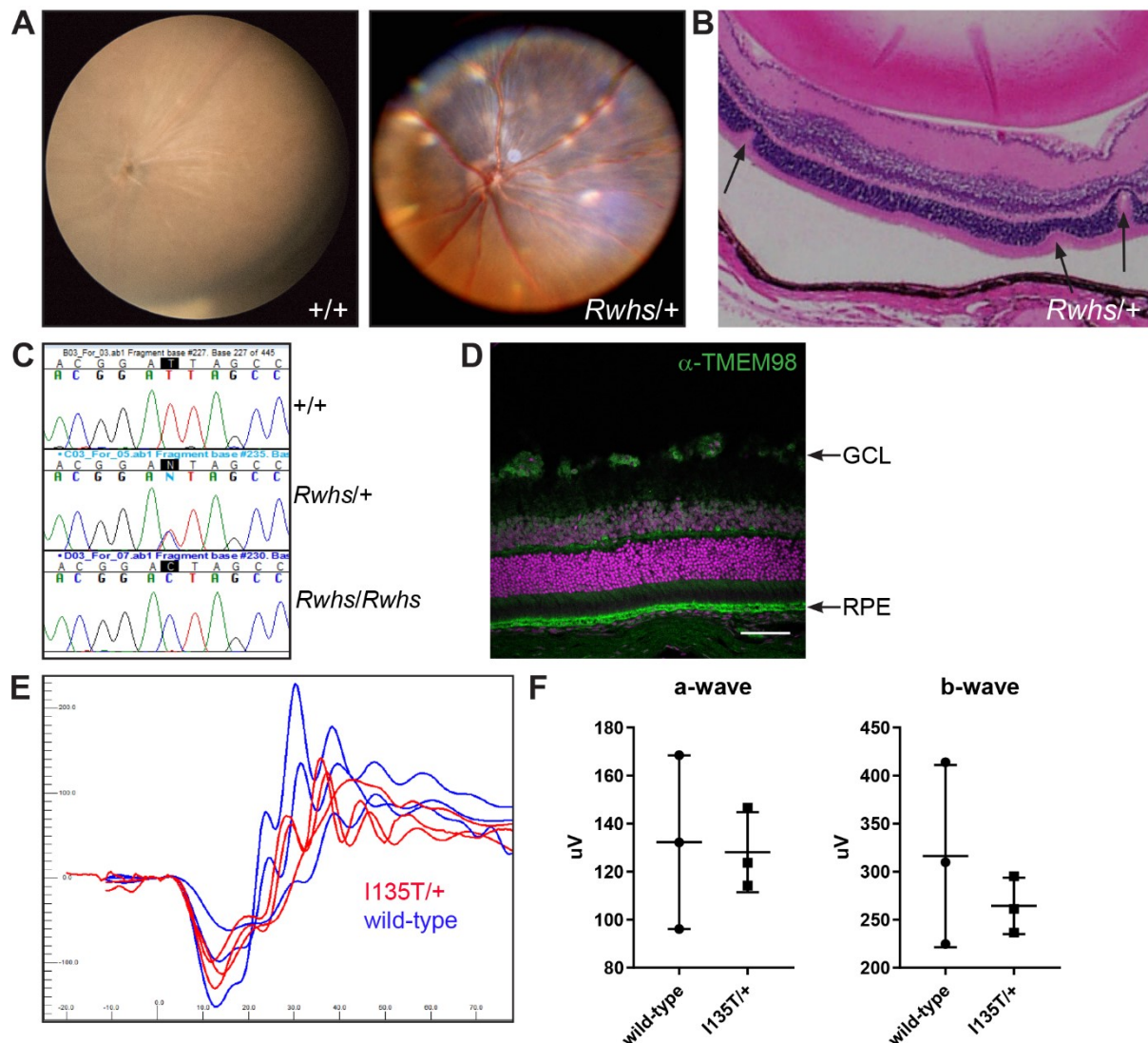
Figures

Figure 1. The *Rwhs* mutation is caused by an I135T mutation of the transmembrane gene *Tmem98*. (**A**) Retinal images of wild-type (+/+) and *Rwhs*/+ eyes. Scattered white spots are present on the *Rwhs*/+ retina. (**B**) *Rwhs*/+ retinal section with three folds in the outer nuclear layer indicated by arrows. The separation of the RPE from the outer segments is a fixation artefact (**C**) Genomic DNA sequence traces from exon 5 of *Tmem98* from wild-type (+/+), heterozygous mutant (*Rwhs*/+) and homozygous mutant (*Rwhs*/*Rwhs*) embryonic samples. The position of the T-to-C transition at position 404 (404T>C) in the coding sequence of *Tmem98* is highlighted. (**D**) A section of wild-type retina immunostained for TMEM98 (green). Prominent staining is seen in the retinal pigment epithelium (RPE) and there is also some staining in the ganglion cell layer (GCL). DNA is shown in magenta. (**E**) *Tmem98*[I135T/+] mice have a normal ERG response. Shown are the responses at 3 cd.s/m^2 (average of 4

21

658   flashes) for the left eye of three *Tmem98^{I135T/+}* mice (5-6 months of age) in red and three

659   wild-type mice (5 months of age) in blue. (**F**) Comparison of a-wave amplitudes (right) and b-

660   wave amplitudes (left), average of left and right eye for each mouse. There is no significant

661   difference between *Tmem98^{I135T/+}* and wild-type mice (a-wave, unpaired t test with Welch's

662   correction, P = 0.87 and b-wave, unpaired t test with Welch's correction, P = 0.45).Scale bar:

663   100 µM (**D**).

664

665
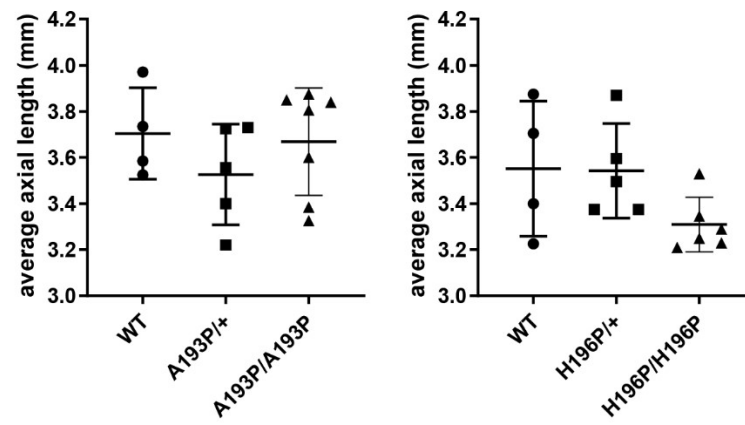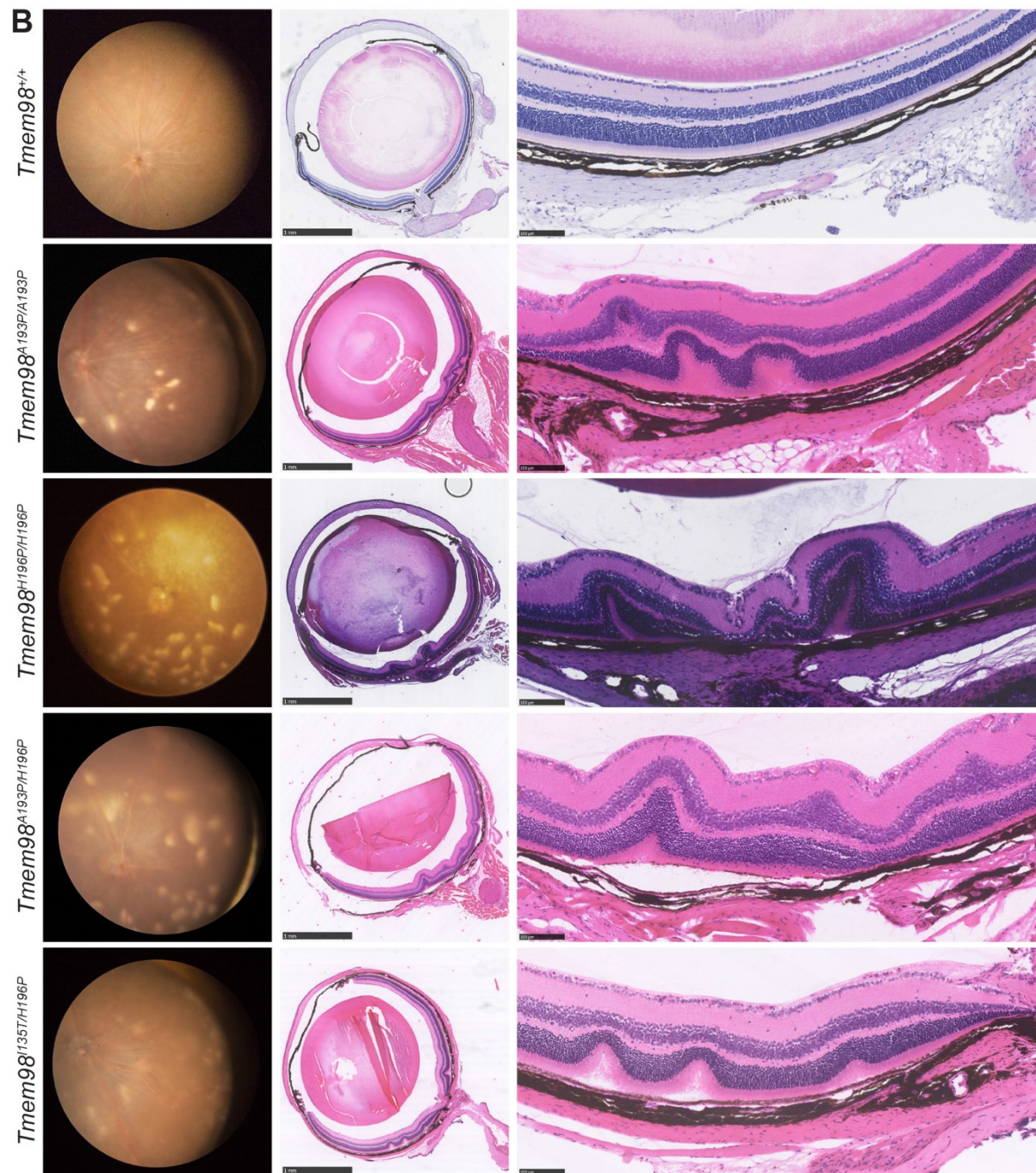
666 **Figure 2.** Eye phenotypes of homozygous and compound heterozygous mice with missense

667 mutations of *Tmem98*. (**A**) Axial length measurements. Shown are the average axial length

668 measurements for each mouse. (**B**) Left panel, retinal images; centre panel sections

669 through the optic nerve; right panel, higher magnification pictures of the retina.

670 *Tmem98$^{A193P/A193P}$* , *Tmem98$^{H196P/H196P}$* ,*Tmem98$^{A193P/H196P}$* and *Tmem98$^{I135T/H196P}$* retinas all

671 have scattered white spots (left panel) and folds in the outer nuclear layer and sometimes

672 the inner retinal layers as well (centre and right panels). Scale bars: 1 mm (**B**, centre panel),

673 100 µM (**B**, right panel).

674

675

676
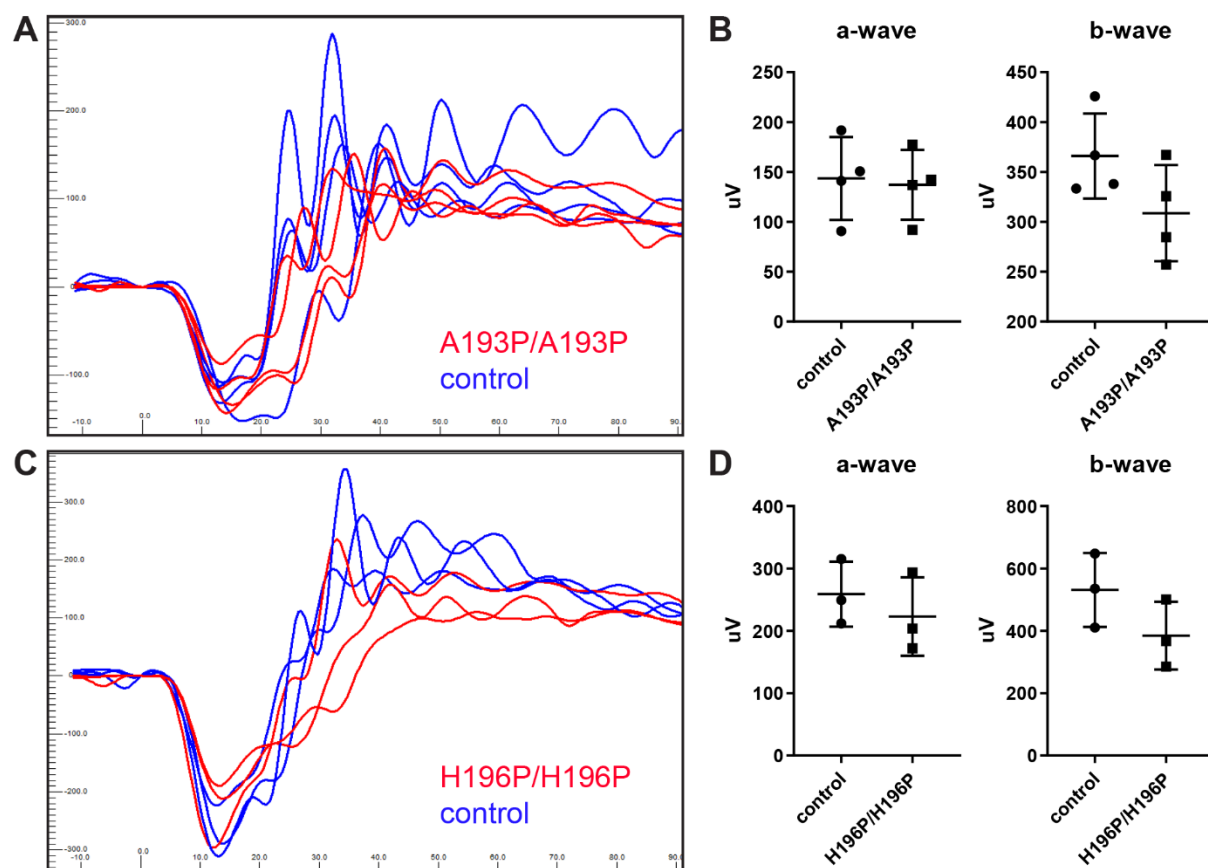
Figure 3. *Tmem98[A193P/A193P]* and *Tmem98[H196P/H196P]* mice have a normal ERG response. (**A-B**) Littermates, four *Tmem98[A193P/A193P]* mice and four control mice (two wild-type and two *Tmem98[A193P/+]*) were tested at four months of age. (**A**) ERG traces of *Tmem98[A193P/A193P]* mice (red lines), and control mice (blue lines). Shown are the responses at 3 cd.s/m^2 (average of 4 flashes) for the left eye. (**B**) Comparison of a-wave amplitudes (right) and b-wave amplitudes (left), average of left and right eye for each mouse. There is no significant difference between *Tmem98[A193P/A193P]* and control mice (a-wave, unpaired t test with Welch's correction, P = 0.82 and b-wave, unpaired t test with Welch's correction, P = 0.13). (**C-D**) Three *Tmem98[H196P/H196P]* mice and three control mice (two wild-type and one *Tmem98[H196P/+]*) were tested at 6 months of age. (**C**) ERG traces of *Tmem98[H196P/H196P]* mice (red lines), and control mice (blue lines). Shown are the responses at 3 cd.s/m^2 (average of 4 flashes) for the left eye. (**B**) Comparison of a-wave amplitudes (left) and b-wave amplitudes (right), average of left and right eye for each mouse. There is no significant difference between *Tmem98[H196P/H196P]* and control mice (a-wave unpaired t test with Welch's correction, P = 0.49 and b-waveunpaired t test with Welch's correction, P = 0.19).

25
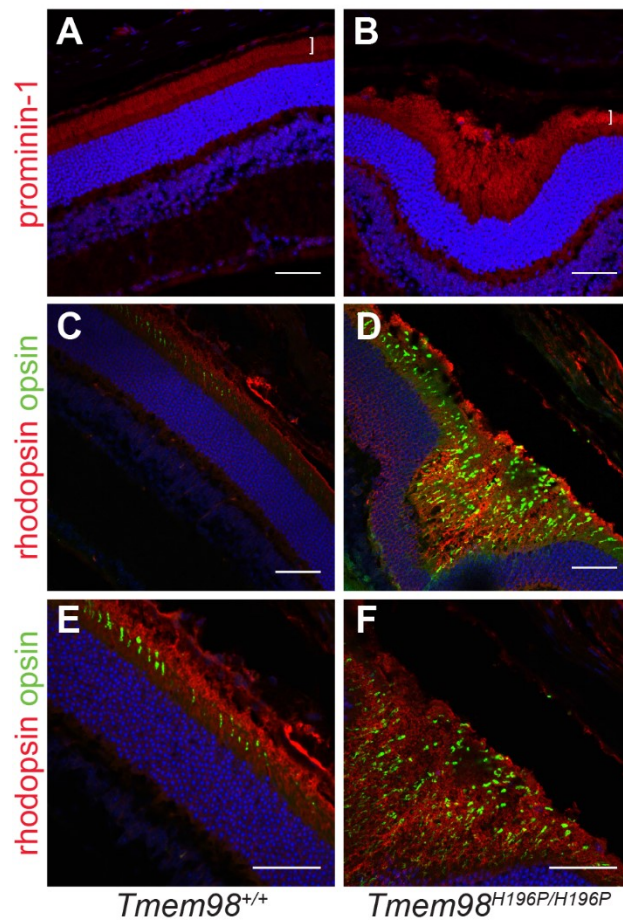
Figure 4. The interiors of the retinal folds found in the *Tmem98*$^{H196P/H196P}$ mutant mice are filled with excess outer segments. Immunostaining of retinal sections from wild-type mice (**A**, **C** and **E**) and *Tmem98*$^{H196P/H196P}$ mice (**B**, **D** and **F**). (**A-B**) Prominin-1 staining (red) shows that the outer segment layer (white bracket) is expanded in the retinal fold of the mutant (**B**) compared to wild-type (**A**). (**C-F**) Rhodopsin (red) and opsin (green) staining shows that the interior of the retinal fold is filled with outer segments. DAPI staining is shown in blue. Scale bars: 50 μM.
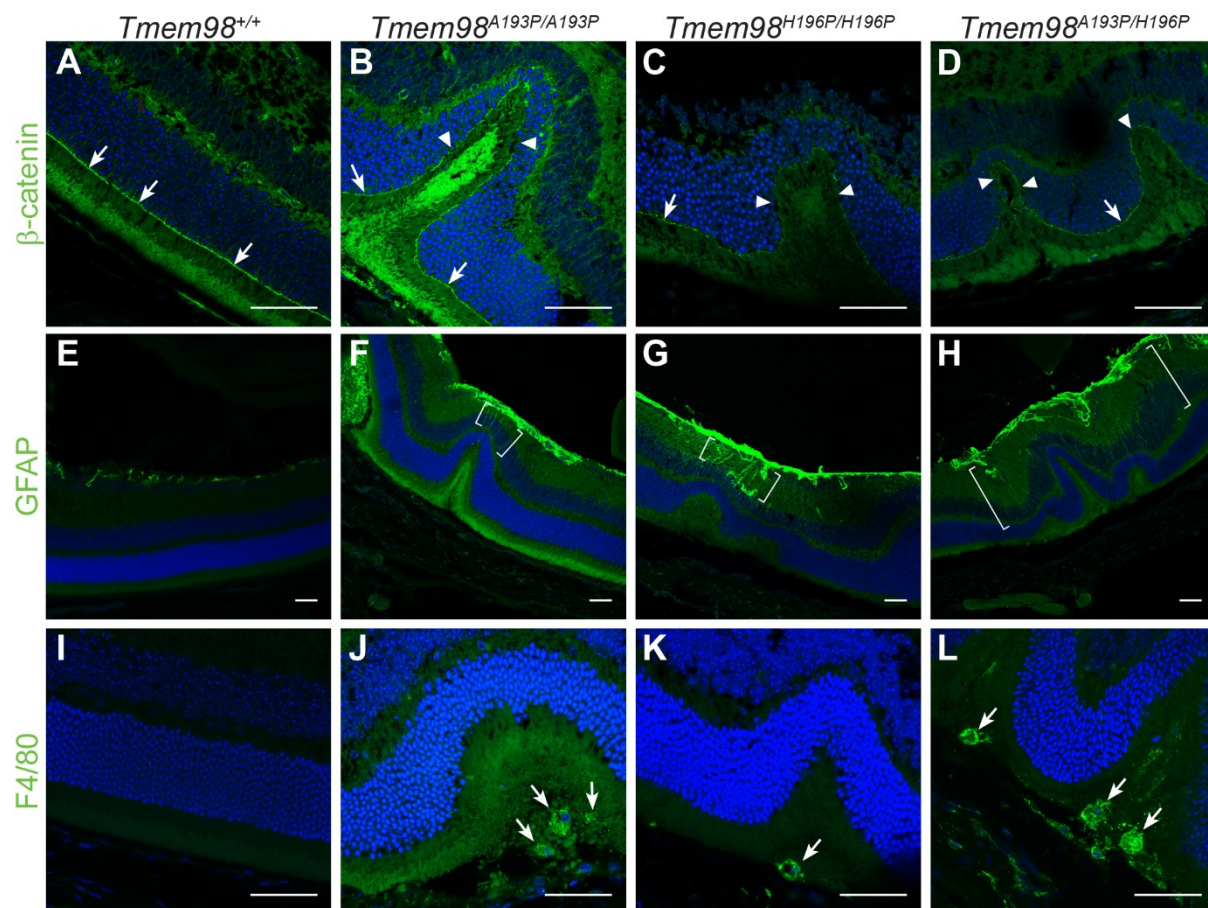
Figure 5. Characterisation of the retinal folds in the *Tmem98* mutant mice. Immunostaining of retinal sections from wild-type mice (**A**, **E** and **I**), *Tmem98*$^{A193P/A193P}$ mice (**B**, **F** and **J**), *Tmem98*$^{H196P/H196P}$ mice (**C**, **G** and **K**), *Tmem98*$^{A193P/H196P}$ mice (**D**, **H** and **L**). (**A-D**) β-catenin staining (green) shows that the OLM is intact in the wild-type retina and in the areas either side of folds in the mutant retinas (white arrows) but in the folds of the mutant retinas the OLM is interrupted (white arrowheads). (**E-H**) GFAP staining (green) is normal in the wild-type retina but above the folds in the mutant retinas there is abnormal GFAP staining extending towards the outer nuclear layer (areas between the white brackets). This indicates that in the mutants the retina is stressed in the folded regions and that retinal stress is confined to the folds. (**I-L**) F4/80 staining (green) reveals that macrophages have infiltrated into the areas below the folded outer nuclear layer containing excess photoreceptors in the mutant retinas (white arrows). Staining was not observed outside the folds in the mutant retinas. DAPI staining is shown in blue. Scale bars: 50 μm.

27
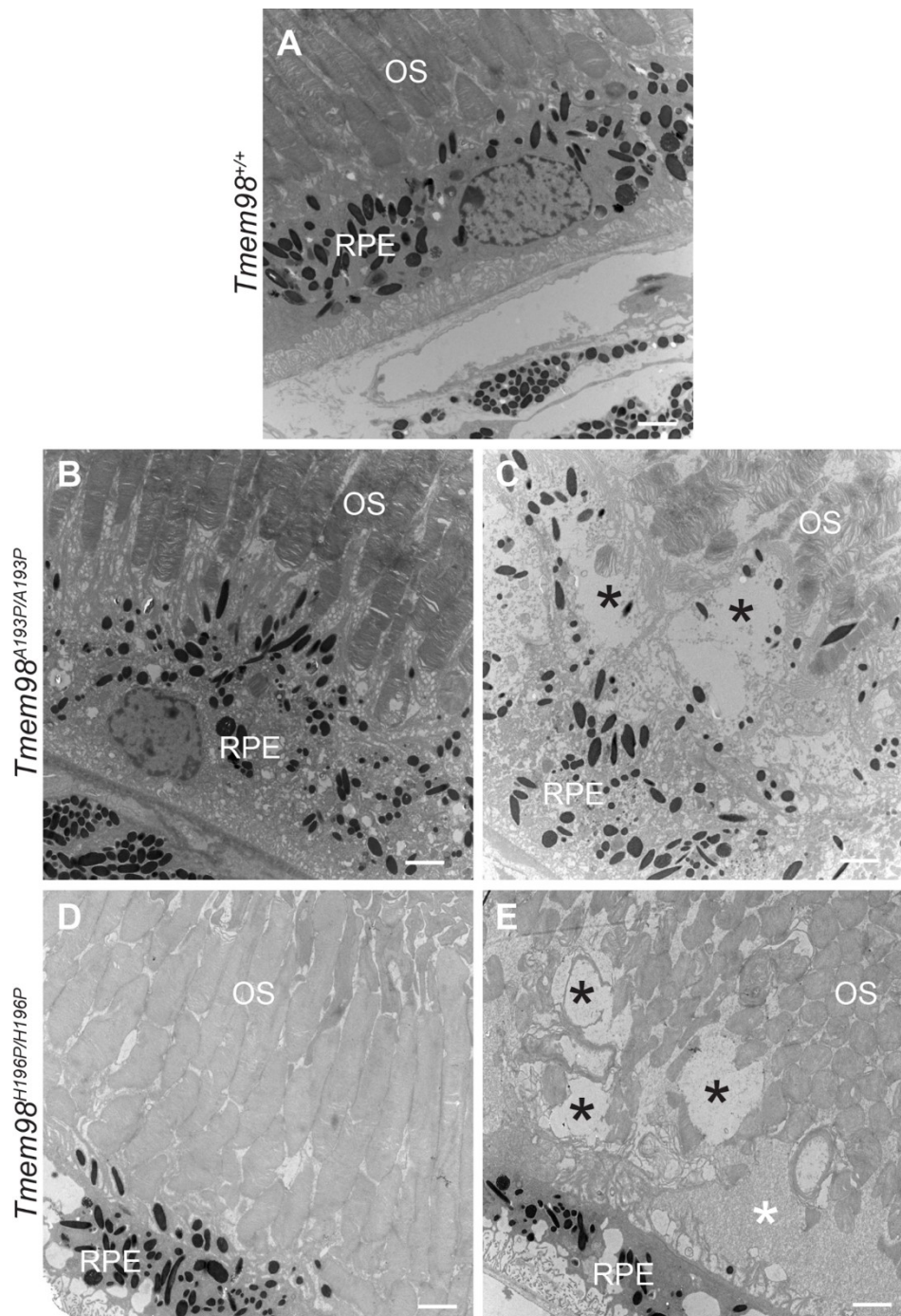
Figure 6. Ultrastructural analysis of the RPE and outer segment boundary. (**A**) Wild-type mice are normal. (**B** and **D**) In mutant mice from retinal regions with no folds the outer segments adjacent to the RPE appear normal. (**C** and **E**) In retinal areas with folds the outer segments abutting the RPE appear abnormal and disorganised. Several large vacuoles (indicated by black asterisks) can be seen. In (**E**) there is an area containing cellular debris (indicated by a white asterisk). $Tmem98^{A193P/A193P}$ (**B**, **C**) and $Tmem98^{H196P/H196P}$ (**D**, **E**). OS = outer segments, RPE = retinal pigment epithelium. Scale bars: 2µm.

28

Figure 7. TMEM98 protein structure and predicted effect of the I135T mutation (**A**) Alignment of TMEM98 proteins (yellow group) and CCNDBP1 proteins (blue group). The

727   positions of predicted α-helices (1-5) are indicated by the curly lines. The positions of the
728   three missense mutations are indicated by the black arrows. (**B**) Helical bundle based upon
729   the crystal structure of CCNDBP1 (c3ay5A). The N- and C-terminal ends are indicated. The
730   region surrounding I135 (dashed box) is enlarged on the right showing the hydrophobic
731   interactions within 5 Å of I135.

Supplementary Methods

Mice

By crossing *Tmem98*^{tm1a/+} mice with mice carrying Flpe the *tm1a* 'knockout-first' allele was converted to a conditional allele *Tmem98*^{tm1c(EUCOMM)Wtsi} (hereafter *Tmem98*^{tm1c}). By crossing *Tmem98*^{tm1c/+} mice with mice carrying Cre the floxed critical exon 4 is deleted generating a deletion allele that has a frame shift *Tmem98*^{tm1d(EUCOMM)Wtsi} (hereafter *Tmem98*^{tm1d}) that would be subject to nonsense mediated decay [39].

Embryonic Protein Preparations

Embryonic day 12.5 (E12.5) embryos were collected and a small piece of tail used for genotyping. Tissue was homogenised in RIPA buffer (Cell Signaling Technology) plus 1 mM phenymethysulfonyl (ThermoFisher Scientific) and Complete Protease Inhibitor Cocktail (Roche) and sonicated for 30s 3 times. Crude lysates were cleared by centrifugation (20,000 g for 30 minutes at 4°C) and protein concentrations determined by Bradford assay (Bio-Rad). 20 µg samples were used for Western blotting.

Western Blotting

Equal amounts of protein lysates were separated on 4-12% Nupage Bis-Tris gels (ThermoFisher Scientific) and transferred to polyvinylidene difluoride or nitrocellulose membranes. Membranes were blocked for one hour at room temperature in SuperBlock T20 (TBS) Blocking Buffer (ThermoFisher Scientific) and incubated with primary antibodies for one hour at room temperature or overnight at 4°C in blocking buffer with shaking. Following washing with TBST membranes were incubated with ECL horse radish peroxidase (HRP)-conjugated secondary antibodies (GE Healthcare) diluted 1:5000 in blocking buffer for one hour at room temperature, washed with TBST and developed using SuperSignal™ West Pico PLUS (ThermoFisher Scientific).

Supplementary Tables

Supplementary Table S1. Sequences of oligos

Oligo Name	Sequence (5'-3')*
ex7_Guide1	CACCGGCCAATCACTGTCTGCCGCTG
ex7_Guide2	AAACCAGCGGCAGACAGTGATTGGCC
A193P	AACCGCCCTGCTGCTGTCCGTTAGTCACTTGGTGCTAGTGACCAGGA ACGCCTGCCATCTAACCGGGGGCCTGGACTGGATTGACCAATCACT GTCTGCC*C*CTGAaGAGCACCTGGAAGTCCTTCGAGAGGCAGCCCTG GCTTCTGAGCCAGATAAAAGCCTCCCCAACCCTGAGGGCTTCCTGCA GGAACAGTCGGCCA
H196P	AACCGCCCTGCTGCTGTCCGTTAGTCACTTGGTGCTAGTGACCAGGA ACGCCTGCCATCTAACCGGGGGCCTGGACTGGATTGACCAATCACT GTCTGCCGCTGAaGAGC*C*CCTGGAAGTCCTTCGAGAGGCAGCCCTG GCTTCTGAGCCAGATAAAAGCCTCCCCAACCCTGAGGGCTTCCTGCA GGAACAGTCGGCCA

*For the repair oligos base changes introducing amino acid changes are underlined and silent base changes destroying the PAM site are in lower case. In the A193P line only the mutation causing the A193P change was found, in the H196P line both base changes were incorporated.

Supplementary Table S2. Genotyping primers

Primer Name	Sequence (5'-3')	Product size/allele information
ex5F	CTTTCCACCCCATTTCCTCT	501 bp (sequenced for $Tmem98^{I135T}$
ex5R	AGGCTCTGTCAGCCCAGTTA	genotyping)
ex7F	CTTGGTGCTAGTGACCAGGA	228 bp (sequenced for $Tmem98^{A193P}$
ex7R	ACAGGAAGTAGAAGGCTCGC	and $Tmem98^{H196P}$ genotyping)
1532	CCAAAGGGGTGCATTTGAAG	465 bp (WT)
1533	TGCAAACCCAAGTCAAAAAGC	595 bp (*tm1c*)
1532	CCAAAGGGGTGCATTTGAAG	196 bp (*tm1a*, *tm1b*, *tm1c*, *tm1d*)
1490	TCGTGGTATCGTTATGCGCC	
LacZF	ATCACGACGCGCTGTATC	108 bp (*tm1a*, *tm1b*)

32

LacZR	ACATCGGGCAAATAATATCG	
1604	CCCCCTGAACCTGAAACATA	310 bp (*tm1b*)
838	CTCAGACACCCAGCCTTCTC	
1605	ACCCTTCTCTCCCTAAGTAGTCT	867 bp (WT)
1606	CCCCAAGCCGTCCTTTCC	1030 bp (*tm1c*)
		238 bp (*tm1d*)
FLPeF	AGGGTGAAAGCATCTGGGAGA	~400 bp (Flpe)
FLPeR	TCAACTCCGTTAGGCCCTTCA	
747	CCTGGAAAATGCTTCTGTCCG	4 primer reaction
748	CAGGGTGTTATAAGCAATCCC	290 bp (control product)
749	AACACACACTGGAGGACTGGCTA	450 bp (Cre)
750	CAATGGTAGGCTCACTCTGGGAG	

767

768

769 **Supplementary Table S3. *Tmem98^tm1a/+*** **intercross genotyping results**

Age	WT	*tm1a/+*	*tm1a/tm1a*	Total	P*
at weaning	21	38	0	59	<0.0001
E16.5-E17.5	10	20	10	40	1.0000

770 *Test for significance using chi-square test

771

33

772 **Supplementary Table S4. Mouse homologues of the human missense nanophthalmos *TMEM98* mutations intercross genotyping**

773 **results at weaning**

Cross	WT	A193P/+	A193P/A193P	H196P/+	H196P/H196P	A193P/H196P	Total	P*
A193P/+ x A193P/+	10	21	12	N/A	N/A	N/A	43	0.9006
H196P/+ x H196P/+	68	N/A	N/A	94	49	N/A	211	0.0516
A193P/+ x H196P/+	23	18	N/A	20	N/A	14	75	0.5164

774 *Test for significance using chi-square test
775 N/A=not applicable

Supplementary Figures
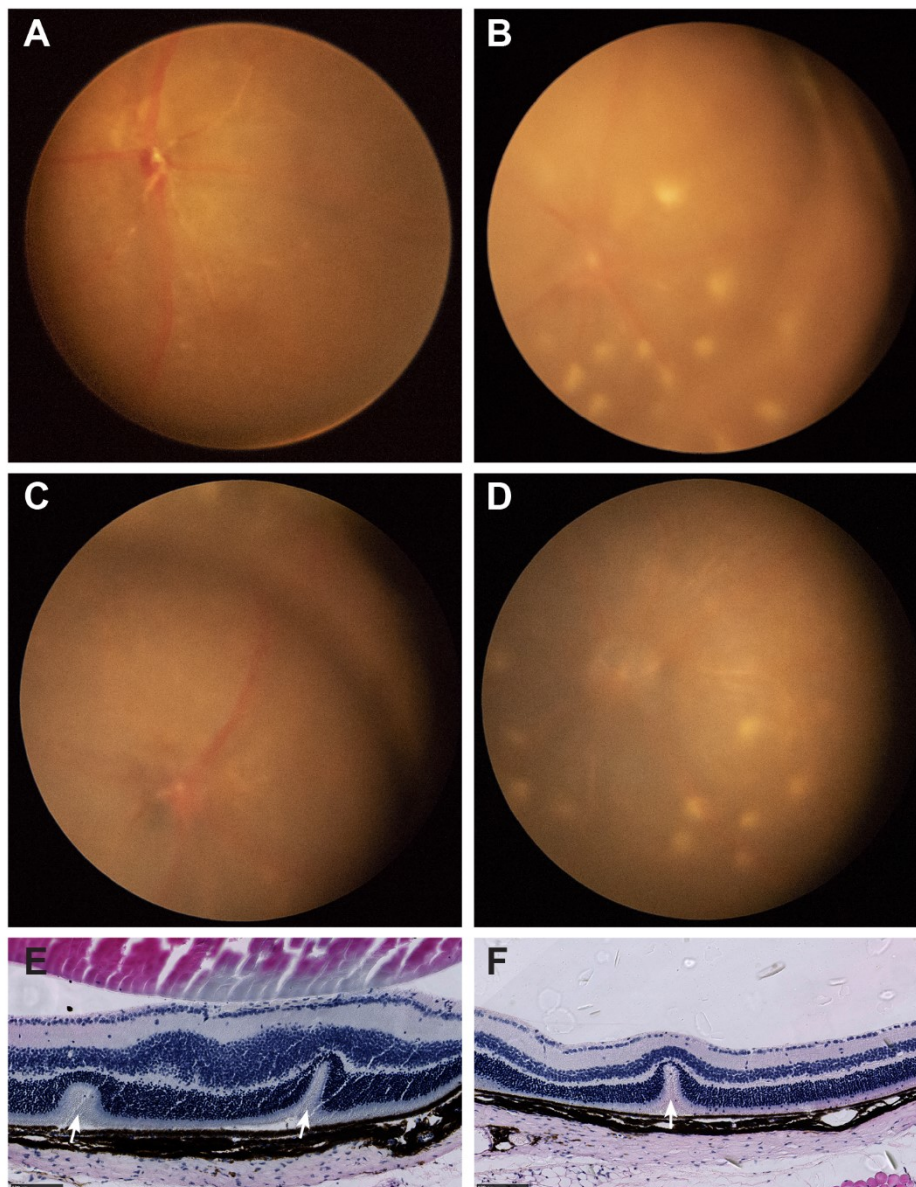
Supplementary Figure S1. Effect of genetic background on the *Rwhs* dominant retinal phenotype. (**A-D**) Retinal images of *Tmem98*$^{135T/+}$ mice on the C57BL/6J genetic background. **A** and **B** are littermates and **C** and **D** are littermates. The mice shown in **A** and **C** have normal retinas whereas the mice shown in **B** and **D** have white spots on their retinas. (**E-F**) Haematoxylin and eosin stained sections of *Tmem98*$^{135T/+}$ retinas on the CAST strain background displaying invaginations of the outer nuclear layer indicated by arrows. Scale bars: 100 μm.

```
CLUSTAL O(1.2.4) multiple sequence alignment

|Q9Y2Y6|TMM98_HUMAN            METVVIVAIGVLATIFLASFAALVLVCRQRYC--RPRDLLQRYDSK-----PIVDLIGAM 53
|Q91X86|TMM98_MOUSE            METVVIVAIGVLATIFLASFAALVVVCRQRYC--RPRDLLQRYDSK-----PIVDLIGAM 53
|Q6AYS5|TMM98_RAT             METVVIVAIGVLATIFLASFAALVVVCRQRYC--RPRDLLQRYDSK-----PIVDLIGAM 53
|Q6INX1|TMM98_XENLA          METVVIVAIGVLATIFLASFAALVVVCRQRYC--RTKNLLTNYNNK-----PTVDLIGAM 53
|Q2HJB9|TMM98_BOVIN          METVVIVAIGVLATIFLASFAALVVVCRQRYC--RPRDLLQCYDSK-----PIVDLIGAM 53
|A1L279|A1L279_DANRE         METVVIVAIGVLATIFLASFVALVVVCRHRYC--HPPDFLHQFDSK-----PTVDLIGAM 53
|A0A1D5PUC5|A0A1D5PUC5_CHICK METVVIVAIGVLATIFLASFVALVVVCRQRYC--RPKDLLHPYDTK-----PIVDLIGAM 53
|H2UZU1|H2UZU1_TAKRU         METVVIVAIGVLATIFLASFVALVVVCRHRYC--HPHHLLHHFDSK-----PTVDLIGAM 53
|H2XZ57|H2XZ57_CIOIN         METVVIVAVSILGVVFVASLVTLLIICRQKYRLCRRHHSILSDNDDDEGSSETVVRVGNN 60
                             ********:..:*..:*:**:..:*:::**::*   :  . :  : .     *  :*

|Q9Y2Y6|TMM98_HUMAN            ETQSEPSELELDDVVITNPHIEAILENEDWIEDASGLMSHCIAILKICHTLTEKLVAMTM 113
|Q91X86|TMM98_MOUSE            ETQSEPSELELDDVVITNPHIEAILENEDWIEDASGLMSHCIAILKICHTLTEKLVAMTM 113
|Q6AYS5|TMM98_RAT             ETQSEPSELELDDVVITNPHIEAILENEDWIEDASGLMSHCIAILKICHTLTEKLVAMTM 113
|Q6INX1|TMM98_XENLA          ETQSEPSDLELDDVVITNPHIEAILEDEDWIEDASGLVSHCIAILKICHTLTEKLVAMTM 113
|Q2HJB9|TMM98_BOVIN          ETQSEPSELELDDVVITNPHIEAILENEDWIEDASGLMSHCIAILKICHTLTEKLVAMTM 113
|A1L279|A1L279_DANRE         ETQSEPSELELDDVVITNPHIEAMLENEDWIEDASGLVSHCIAILKICHTLTEKLVAMTM 113
|A0A1D5PUC5|A0A1D5PUC5_CHICK ETQSEPSELELDDVVITNPHIEAILENEDWIEDCVPTLSPL---PSGGRGGGEKLVAMTM 110
|H2UZU1|H2UZU1_TAKRU         ETQSEPSELELDDVVITNPHIEAILENEDWIEDASGLVSHCISILKICHTLTEKLVAMTM 113
|H2XZ57|H2XZ57_CIOIN         AN----ENHIQSTITFDDGTIRHLLETEDWANDIHGLVPHCIAILKMCREVTEKLVALTL 116
                             .    .:    . :.: :  *. :** *** :*     :        .  :   *****:*:

|Q9Y2Y6|TMM98_HUMAN            GSGAKMKTSASVSDIIVVAKRISPRVDDVVKSMYPPLDPKLLDARTTALLLSVSHLVLVT 173
|Q91X86|TMM98_MOUSE            GSGAKMKTSASVSDIIVVAKRISPRVDDVVKSMYPPLDPKLLDARTTALLLSVSHLVLVT 173
|Q6AYS5|TMM98_RAT             GSGAKMKTSASVSDIIVVAKRISPRVDDVVKSMYPPLDPKLLDARTTALLLSVSHLVLVT 173
|Q6INX1|TMM98_XENLA          GSGAKMKSPSSLSDIIIVAKRISPRVDDVVRSMYPPLDPKLLDARTTALLLSVSHLVLVT 173
|Q2HJB9|TMM98_BOVIN          GSGAKMKTSASLSDIIVVAKRISPRVDDVVKSMYPPLDPKLLDARTTALLLSVSHLVLVT 173
|A1L279|A1L279_DANRE         GSGAKVKAPASLNDIITVAKRISPRVDDVVRSMYPPLDPILLDARATALLLSVSHLVLVT 173
|A0A1D5PUC5|A0A1D5PUC5_CHICK GSGARAKSPSSLGDIIVVAKRISPRVDDVVRSMYPPLDPKLLDARAAALLLSVSHLVLVA 170
|H2UZU1|H2UZU1_TAKRU         GSGAKVKAPASLSDIITVAKRISPRVDDVVRSMYPPLDPILLDARATALLLSVSHLVLVT 173
|H2XZ57|H2XZ57_CIOIN         DRKQENVQSSDMAIIVGVAKRITPRVDDVISSIAPPLNPISLESKCSALIYSVQHLAILV 176
                             .   .   :.:  *: *****:******: *: ***:*  *::: :**: **.**.::.

|Q9Y2Y6|TMM98_HUMAN            RNACHLTGGLDWIDQSLSAAEEHLEVLREAALASEPDKGLPGPEGFLQEQSAI 226
|Q91X86|TMM98_MOUSE            RNACHLTGGLDWIDQSLSAAEEHLEVLREAALASEPDKSLPNPEGFLQEQSAI 226
|Q6AYS5|TMM98_RAT             RNACHLTGGLDWIDQSLSAAEEHLEVLREAALASEPDKSLPNPEGFLQEQSAI 226
|Q6INX1|TMM98_XENLA          KNACHLTGGMDWIDQSLSAAEDHLAVLREAALATEPERPMTGADNFLQEQSAI 226
|Q2HJB9|TMM98_BOVIN          RNACHLTGGLDWIDQSLTAAEEHLEVLREAALASEPDKGLPGPEGFLQEQSAI 226
|A1L279|A1L279_DANRE         RNACHMSGSLDWIDQSLHAAEDHMVVLREAALASEPERCFPDREQSI------ 220
|A0A1D5PUC5|A0A1D5PUC5_CHICK RSACPQPGDRDWVDRSLAAAEQHMAALRHAAMATEPERSAA-AEPFRQEQSAI 222
|H2UZU1|H2UZU1_TAKRU         RNACHMSGSLDWIDQSLHAAEDHMVVLREAALASEPERSLPGADAQREQAI-- 224
|H2XZ57|H2XZ57_CIOIN         RKAWQSTGSLEWIDIAFDTMADHMRIISSARYYPQVSQHNNKPDVDANAESSQ 229
                             :.*    *. :*:* :: :  :*:  :  *    : .:      :
```

Supplementary Figure S2. TMEM98 protein sequences from different species aligned using the Clustal Omega program. The uniprot accession numbers and identifiers are shown on the left. An * indicates a completely conserved residue, a : indicates that residues have strongly similar properties (scoring > 0.5 in the Gonnet PAM 250 matrix), a . indicates that residues have weakly similar properties (scoring =< 0.5 in the Gonnet PAM 250 matrix). I135, which is mutated in *Rwhs*, is completely conserved and highlighted in red. The two residues affected in the human nanophthalmos patients, A193 and H196, are highlighted in green. Both are completely conserved except that a methionine is substituted for A193 in *Ciona intestinalis*.

Supplementary Figure S3. TMEM98 protein is expressed in the missense mutants. (**A**) Western blot analysis of E12.5 embryonic protein lysates of the indicated genotypes. TMEM98 protein can be detected in the wild-type and heterozygous samples but not the homozygous knock-out samples validating the antibody. (**B**) Western blot analysis of E12.5 embryonic protein lysates of the indicated genotypes. TMEM98 is present in the homozygous mutants carrying the missense mutations found in human nanophthalmos patients. Alpha tubulin was used as a loading control.

805
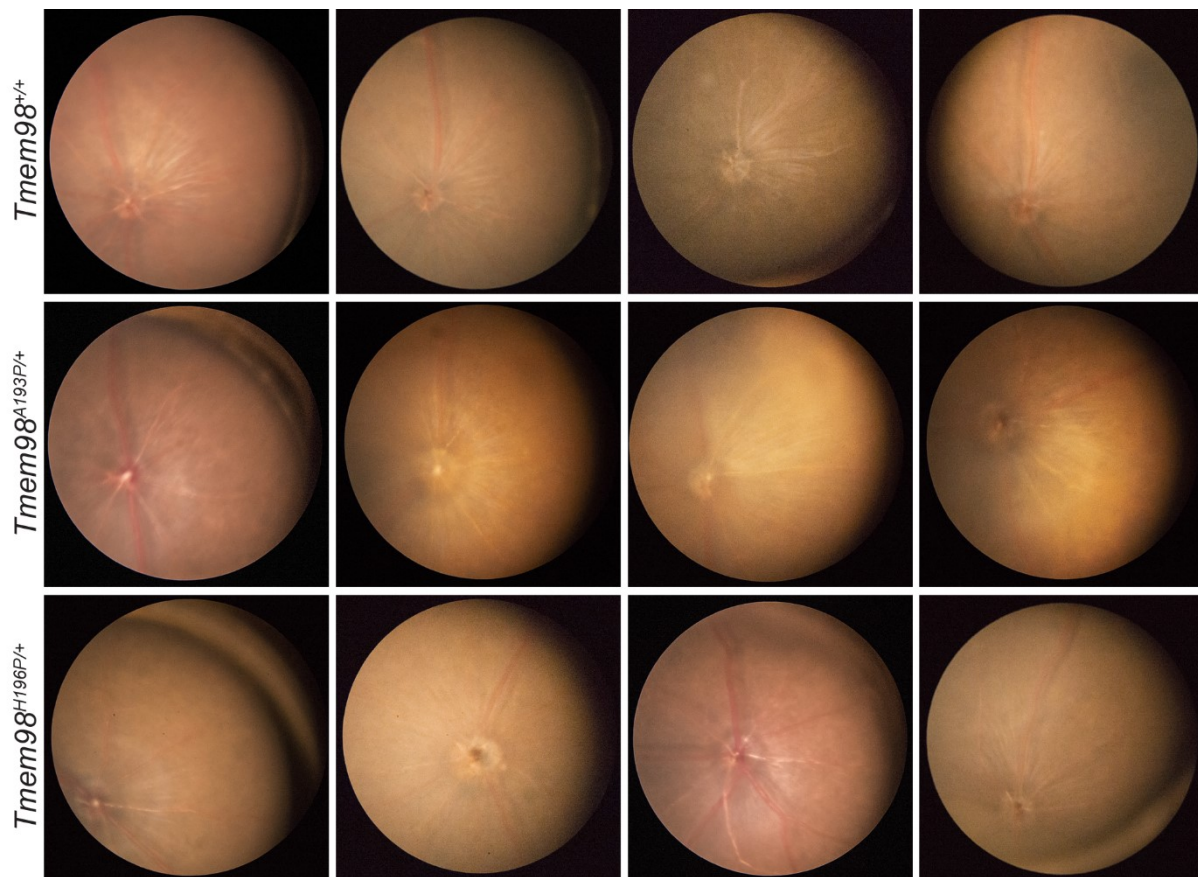
Supplementary Figure S4. Retinas of mice heterozygous for the human nanophthalmos missense mutations are normal. Retinal pictures from mice of between 5-10 months are shown. Top row wild-type mice, middle row $Tmem98^{A193P/+}$ mice and bottom row $Tmem98^{H196P/+}$ mice.

810
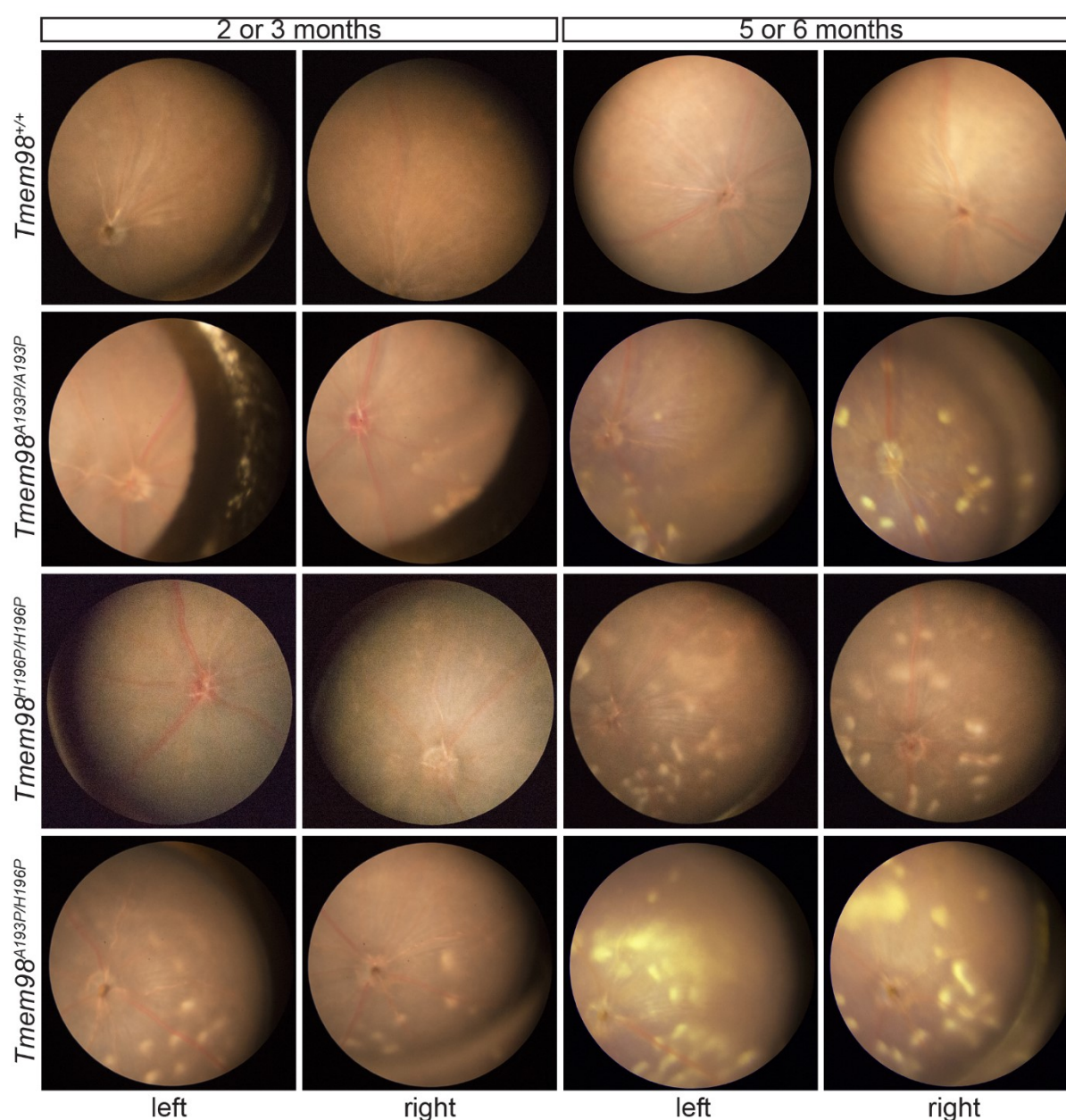
Supplementary Figure S5. The retinal white spotting recessive phenotype in mice carrying the human nanophthalmos missense mutations is progressive. Retinal pictures of the left and right eyes of mice taken at the indicated ages. First row wild-type, second row *Tmem98^{A193P/A193P}*, third row *Tmem98^{H196P/H196P}* and fourth row *Tmem98^{A193P/H196P}*. The wild-type eyes have normal retinas at 5 months. On *Tmem98^{A193P/A193P}* retinas only a few spots are present at 3 months but there is extensive spotting at six months. The *Tmem98^{H196P/H196P}* retinas appear normal at 3 months but there is extensive spotting at six months. On *Tmem98^{A193P/H196P}* retinas a few spots are present at 2 months but there is extensive spotting at 5 months.

820
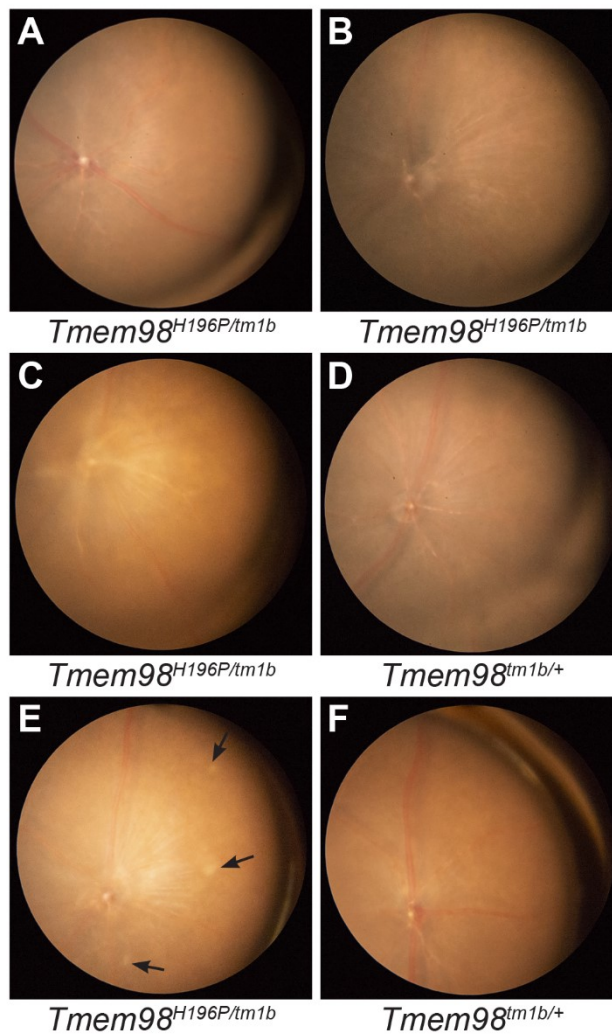
Supplementary Figure S6. *Tmem98$^{H196P/tm1b}$* retinas rarely have retinal white spots. Retinal pictures of *Tmem98$^{H196P/tm1b}$* mice (**A**-**C** and **E**) and *Tmem98$^{tm1b/+}$* mice (**D** and **F**). The retinas shown in **E** and **F** are from littermates. *Tmem98$^{tm1b/+}$* retinas are normal. *Tmem98$^{H196P/tm1b}$* retinas are normal except for the one shown in **E** at one year of age which has three faint white spots indicated by arrows.

826
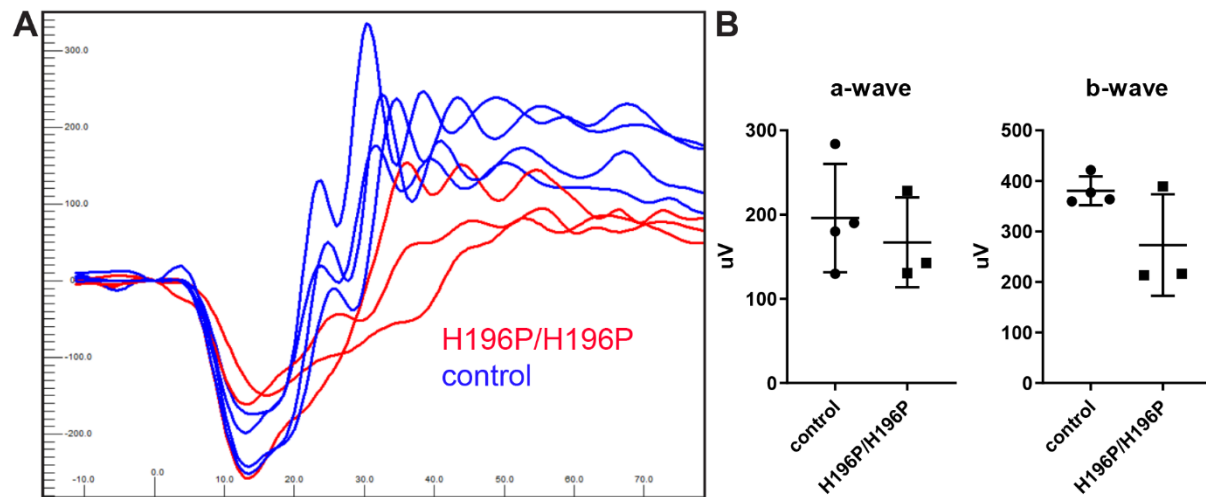
Supplementary Figure S7. ERG response of $Tmem98^{H196P/H196P}$ mice at 9-11 months of age is normal. Three $Tmem98^{H196P/H196P}$ mice (two at 11 months of age and one at 9 months of age) and four 11 month old control mice (three $Tmem98^{H196P/+}$ and one wild-type) were tested. (**A**) ERG traces of $Tmem98^{H196P/H196P}$ mice (red lines), and control mice (blue lines). Shown are the responses at 3 cd.s/m^2 (average of 4 flashes) for the right eye. (**B**) Comparison of a-wave amplitudes (left) and b-wave amplitudes (right) , average of left and right eye for each mouse. There is no significant difference between $Tmem98^{H196P/H196P}$ and control mice (a-wave, unpaired t test with Welch's correction, P = 0.55 and b-wave, unpaired t test with Welch's correction, P = 0.20).

836

41

837
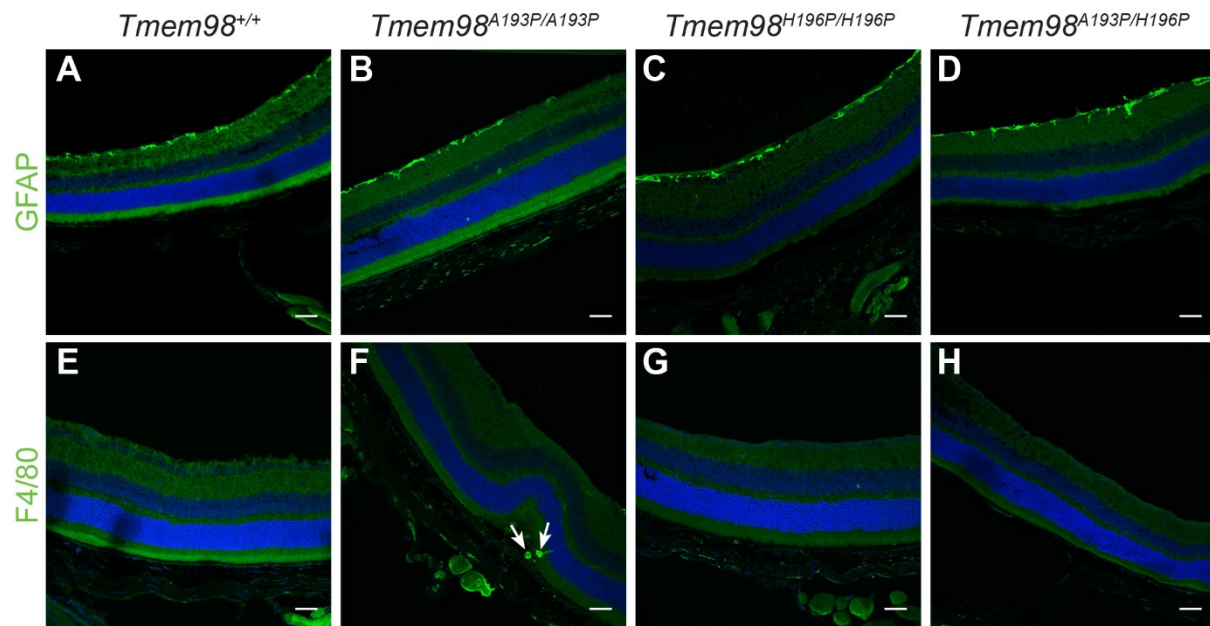
Supplementary Figure S8. GFAP and F4/80 is normal outside the areas with retinal folds in the mutants. Immunostaining of retinal sections from wild-type mice (**A** and **E**), *Tmem98$^{A193P/A193P}$* mice (**B**, and **F**), *Tmem98$^{H196P/H196P}$* mice (**C** and **G**), *Tmem98$^{A193P/H196P}$* mice (**D** and **H**). (**A-D**) GFAP staining (green) is normal for all genotypes. GFAP is expressed in the ganglion cell layer where it is principally found in astrocytes. (**E-H**) F4/80 staining (green) was not observed outside the folds in the mutant retinas. The white arrows indicate macrophages within a fold in the outer segments for *Tmem98$^{A193P/H196P}$*. (**F**) DAPI staining is shown in blue. Scale bars: 50 µm.